Impact microcrater morphology on Australasian microtektites

M. Shyam PRASAD[*] and V. D. KHEDEKAR

Geological Oceanography Division, National Institute of Oceanography, Dona Paula, Goa–403004, India
[*]Corresponding author. E-mail: shyam@darya.nio.org

Abstract–Scanning electron microscopy of 137 Australasian microtektites and fragments from 4 sediment cores in the Central Indian Ocean reveals more than 2000 impact-generated features in the size range of 0.3 to 600 μm. Three distinct impact types are recognized: destructive, erosive, and accretionery. A large variation in impact energy is seen in terms of catastrophic destruction demonstrated by fragmented microtektites through erosive impacts comprising glass-lined pit craters, stylus pit craters, pitless craters, and a small number of accretionery features as well. The size range of observed microtektites is from 180 to 2320 μm, and not only are the smaller microtektites seen to have the largest number of impacts, but most of these impacts are also of the erosive category, indicating that target temperature is an important factor for retaining impact-generated features. Further, microcratering due to collisions in impact-generated plumes seems to exist on a larger and more violent scale than previously known. Although the microcraters are produced in a terrestrially generated impact plume, they resemble lunar microcraters in many ways: 1) the size range of impacts and crater morphology variation with increasing size; 2) dominant crater number densities in μm and sub-μm sizes. Therefore, tektite-producing impacts can lead to the generation of microcraters that mimic those found on lunar surface materials, and for the lunar rocks to qualify as reliable cosmic dust flux detectors, their tumbling histories and lunar surface orientations have to be known precisely.

INTRODUCTION

The microcraters on the Moon are produced mainly by interplanetary dust particles impacting on an atmosphereless Moon and have a size range of <0.1 μm to a few cm (Neukum et al. 1972; Horz et al. 1971, 1991). These craters, found ubiquitously on lunar rocks, breccia, and spherules, have been very important cosmic dust detectors and have also been useful in making fine distinctions regarding the size distribution of meteoroids at 1 AU (Horz et al. 1975). Further, lunar microimpact studies have also made important contributions to our understanding of the mass distribution of meteoroids in interplanetary space (e.g., Brownlee et al. 1975). All interpretations in understanding the microimpact phenomena have been made possible by simulation experiments, which provided the parameters regarding the impacting particle sizes, projectile velocities, and resultant crater geometries (e.g., Vedder 1971; Vedder and Mandeville 1974; Neukum et al. 1972; Fechtig et al. 1978; Bloch et al. 1971; and others).

A wide range of crater geometry has been identified on lunar surface materials (Horz et al. 1971; Schneider and Horz 1974). All microcrater population studies have observed a dominance of sub-μm/few μm-size craters on the specimens studied, and the crater morphology changed with increasing diameter (e.g., Morrison et al. 1973; Hartung et al. 1972).

In addition to the lunar microcraters, Australasian microtektites have been the only natural specimens that recorded impact microcraters in large numbers (Prasad and Sudhakar 1996, 1998). These studies have shown that interparticle collisions within an ejecta plume are violent enough to leave their imprint on many microtektites. In these studies, however, the emphasis for the identification of impact has been accretionary features and melt (Prasad and Sudhakar 1998). This imparted a selection bias in the identification of genuine hypervelocity craters (i.e., those with a central glass-lined pit, radial, and concentric cracks).

In this study, we examined 3404 Australasian microtektites from 4 sediment cores in the Indian Ocean having a diameter range of 180–2320 μm for impact features. We carried out detailed SEM investigations on 137 microtektites and fragments and identified over 2000 impact-generated features. The range of impact-generated features found on Australasian microtektites is presented here. In many ways, these features appear similar to those found on lunar materials.

MATERIALS AND METHODS

Microtektites from 4 sediment cores recovered from the Central Indian Ocean basin during the fourth cruise of Akademik Aleksandr Sidorenko (research vessel chartered by the Government of India) are used here (Table 1). The microtektites from these cores have been identified as belonging to the Australasian tektite strewn field by virtue of their physical appearance, geographic location, and stratigraphic positions. The microtektites were isolated from the sediments in 2 size fractions: >250 µm and 125–250 µm. Standard methods were followed for processing the sediment cores (Glass and Zwart 1979). In all, 3404 microtektites were recovered from these 4 cores in both of the above size fractions.

The microtektites were first scanned with a binocular microscope (magnification up to 50×) for impact-generated features, and subsequently, 137 impacted microtektites and fragments were examined in a JEOL JSM-5800LV scanning electron microscope. Magnifications up to 35000× were used to identify the smallest possible crater, and about 1300 SEM images were obtained covering the range of impacts. Also, while it was easier to recognize impact-generated features in the larger, smoother microtektites, an attempt was made to scan the smaller and also some of the apparently rough microtektites in this study (the smallest impacted microtektite observed in our earlier study had a diameter of 590 µm; Prasad and Sudhakar 1998). This resulted not only in a lower average size of the impacted microtektites (Table 2), but also,

more than an order of magnitude higher number of impacts are observed. Further, 6 microtektites in the size class 125–250 µm and 2 having diameters ~260 µm from core AAS 4/1 are also included in the present study.

BINOCULAR MICROSCOPE OBSERVATIONS

The microtektites had the shapes, colors, and surface features associated with the Australasian microtektites (Glass 1974). While about 95% of the observed microtektites were spheres, the other shapes seen are dumbbell, club, oval, disc, etc. All of them displayed colors that are variants of white, brown, and green-yellow. The smaller ones are more whitish or colorless.

The microtektities showing microimpact features were separated and their sizes and identifiable impact features were noted. The features on microtektites >250 µm were more easily identifiable, and about 10% of all microtektites in this size fraction contained impact-generated features (Table 1). This is higher than the 6.45% for the same size fraction found earlier (Prasad and Sudhakar 1998).

Recognizing impact-generated features in the 125–250 µm microtektite size class is difficult (although microtektites in this size range are more abundant in all the samples) because there are more "rough" surfaced microtektites in this size range than in the >250 µm size class. Also, considering equal amounts of etching (up to 15 µm; Glass 1984) for all size classes of microtektites, the smaller ones have the disadvantage of undergoing higher amounts of etching for

Table 1. Sampling details of impact phenomena.

| | | Microtektites >250 µm size | | | | | Microtektites 125–250 µm size | |
Sample	Location	Total observed[a]	Microtektites with impacts	No. of fragments	Size range of impacted microtektites (µm)	Average size of impacted microtektites (µm)	Total observed[a]	Fragments
AAS 4/1	11°15.661′ S 75°00.706′ E	445	73	22	300–1400	558	659	52
AAS 4/2	12°00.105′ S 75°29.967′ E	277	19	7	280–1725	666	379	59
AAS 4/5A	12°30.500′ S 76°30.990′ E	401	28	32	370–2000	821	662	102
AAS 4/6	12°36.968′ S 78°30.757′ E	364	30	14	295–2400	810	217	36
Total		1487	150	75			1917	249

[a]Including fragments.

Table 2. SEM observation data of impact phenomena.

| | No. of microtektites observed | | Size range of impacted | Average size of impacted | Average no. of |
Sample	Microtektites	Fragments	microtektites (µm)	microtektites (µm)	impacts/microtektite
AAS 4/1	40	7	181–826	515	26.2
AAS 4/2	24	6	350–1724	624	26
AAS 4/5A	20	9	374–1818	837	13.4
AAS 4/6	22	9	391–2320	834	10
Total	106	31			

their sizes. Interestingly, fragments have been found in both size classes; their percentage is higher in the 125–250 µm sizes (13%).

Some of the problems with identifying impact-generated features using the binocular microscope are:

1. As mentioned above, natural etching by sea water is the primary reason for obliterating or masking impact features on microtektites, while lunar materials are pristine and much easier to characterize. Further, especially among the smaller impact features, distinguishing between etch pits, conchoidal fracturing, and radial and concentric cracks typical of impact is difficult—this can be confirmed only by SEM examination. The small microtektites have the highest number of craters per microtektite (Fig. 1) and are also the most etched ones because of their larger exposed area/mass ratios. If all the craters on the smaller microtekties (125–250 µm) were counted, the total number of craters could easily be an order of magnitude higher than those presented here.

2. The microtektites are isolated from the sediments after wet sieving and drying. Sieving is a mechanical process in which friction could easily dislodge some of the delicate features such as radial cracks, etc. Consequently, sometimes only a central pit is seen; the surrounding radial cracks seem to have been dislodged, exposing the underlying ridges.

3. One criterion, which was found to be reasonably reliable, especially among the smaller microtektites, was to detect microtektites which had at least 1 impact large enough to be identified. However, others exist in which all the impacts are small (<20 µm). Many microtektites that appeared etched under the binocular microscope showed up to be close-spaced or overlapping clusters of craters in the SEM.

SEM OBSERVATIONS

Microtektite Size and Number of Impacts

On the 137 microtektites and fragments investigated in the SEM, a total of 2030 microimpacts have been counted. Microtektite shape does not seem to pose any limitations on the impact phenomena—impacts have been found on spheres, oval shapes, dumbbells, club shapes, and discs (Fig. 2). The host size seems to have an inverse relation not only with the number of impacts, but also with the type of impact (more erosive impacts with decreasing microtektite diameter, as discussed below). The largest microtektite observed here is a 2320 µm-sized dumbbell (sample AAS 4/6), and the smallest is a 180 µm-sized sphere seen in the sample AAS 4/1 (Table 2). Three general size distinctions are observed in this data with respect to the number of impacts on their surfaces (Figs. 1 and 2):

1. The large-sized microtektites having a diameter ≥800 µm contain the least number of impacts/microtektite (<10).

2. Medium-sized microtektites between diameters ~450 to 800 µm show 2 impact populations, i.e., those having <10 impacts and those with a large number of impacts (maximum of 104 impacts on 1 microtektite).

3. The small microtektites with diameters ≤450 µm have the largest number of impacts/microtektite (310 is the highest number of impacts counted on 1 microtektite).

Within the 4 cores studied, the average size of the impacted microtektites decreases from AAS 4/6 through AAS 4/1, but the number of impacts/microtektite increases (Table 2). The average microtektite size in AAS 4/6 is 834 µm, which shows 10 impacts/microtektite, and in AAS 4/1, the average impacted microtektite size is 515 µm and the number of impacts/microtektite is 26. In this sample, 6 microtektites from the 125–250 µm size fractions were observed that contained an average of 32 impacts/microtektite. In AAS 4/2 also, 26 impacts/microtektite are observed, however, 1 specimen alone has 310 impacts, which enhances the average in this sample. If this microtektite were not considered, the average would be 12 impacts/microtektite. Overall, the number of impacts/microtektite has a wide range of 1–310.

Types of Impacts

The impacts are classified into 3 categories: destructive, erosive, and accretionery, generally following the description given by Le Sergeant et al. (1981). Their relative percentages are given in Fig. 3. The above 3 microtektite size classes are also distinct in the type of impacts that are seen on them. The large microtektites mainly show a combination of low-velocity and accretionery impacts. The medium-sized ones have the entire range of impacts: all categories of erosive and accretionery impacts. While the small microtektites mainly show erosive impacts and accretionery impacts, these impacts are rare on these microtektites. Further, the smallest craters (especially the sub-µm-sized craters) are seen only on the small microtektites. Generally, when a large number of impacts are seen on 1 microtektite, the dominant impact type is erosive. Crater diameters ranging from 0.3 to 600 µm are observed.

Destructive Impacts

Le Sergeant et al. (1981) described destructive impacts as impacts where the projectile completely destroys the target because the projectile size approaches target dimensions. Fragments fit into this collisionally-produced category.

Fragments: In all, 31 fragments were selected for observation in the SEM—all of them containing some evidence of impact. Fragments are found in both the >250 µm and 125–250 µm microtektite size categories. The percentage of fragments is, however, higher (13%) in the smaller size category of 125–
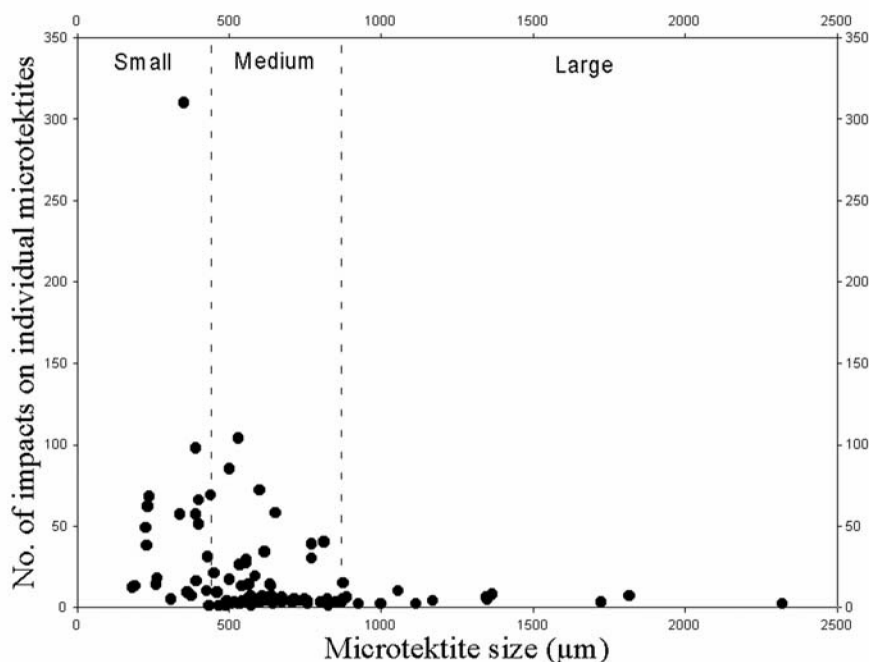
Fig. 1. Microtektite size versus number of impacts on each microtektite.

250 μm (Table 1). Glass et al. (1997) defined fragments as angular pieces of glass that appear to have formed by fragmentation of larger splash forms. The fragment percentage shown by Glass et. al. (1997) in this area ranges from 0–13% of the >125 μm-sized microtektites. Fragments fitting the general description given by Glass et al. (1997) are also seen with a clean break and no evidence of radial and concentric cracks and melt. Those considered to be due to impact are shown here (Fig. 4), and they contain some evidence of impact in the form of a clean break (Figs. 4a and 4b), other craters on the specimen (Fig. 4b), or intense cracks and melt (Fig. 4c). The melt in Fig. 4c indicates either a target/projectile that was hot or was produced during the impact event. A spall fragment that is similar to peel offs typical for the antipodal region of destructive collision (Fig. 4d; Horz 1969) is also observed. Dumbbell-shaped microtektites broken by impact, which are similar to the one shown by Prasad and Sudhakar (1998), are also seen. Milder versions of collisions result in suppressed spheres where the cooling is not complete and, therefore, show circumferential cracks in the equatorial regions.

Here, each fragment is considered to be due to 1 destructive impact. Each fragment could also be the result of several impacts adding cumulatively to the reduction of target strength (Gault and Wedekind 1969), and the 31 fragments observed here constitute 8% of the total fragment population (Table 1). If the impact energy exceeds the threshold of 10^7 ergs/g, the host gets fragmented (Gault and Wedekind 1969). We suggest that a certain percentage of the fragments have been collision-induced. Some others can be due to differential cooling upon contact with sea water (Glass et al. 1997). A larger percentage of the fragmented microtektites ends up in the smaller size fractions (125–250 μm), but we have not scanned for microtektites smaller than <125 μm diameter.

Crater Remnants: Crater remnants are individual "pieces" of craters. A majority of these show melt (Fig. 5). Mostly radial and minor concentric cracks are seen on these pieces. The majority of these craters must have originated from large microtektites. Some of them show long needles of melt (Fig. 5d). Invariably, these crater remnants seem to belong to large-sized microtektites. The melt seen on most of these specimens seems to indicate that the impact shattered the hosts while they were still hot.

Protrusions: Although strictly belonging to the erosive category, protrusions are included here because some of them seem to be the consequence of collision between objects of similar sizes, causing a large-scale distorsion of the target shape (Fig. 6). Protrusions are unique to microtektites and were first reported on a microtektite by Prasad and Sudhakar (1996). These are seen at different scales, both requiring essentially a target that is hot. A microtektite collides with an object, the host melts, and part of the melted portion stands out (Fig. 6a). Further, the impact causes a portion of the host to break and stand up as an angular protrusion (Fig. 6b). Two projections are seen on some hosts (Figs. 6a and 6b). Further, a large-scale collision causes shape distorsion of the host where at least half of the microtektite is "pushed" out, accompanied by melt and schlieren (Fig. 6c).
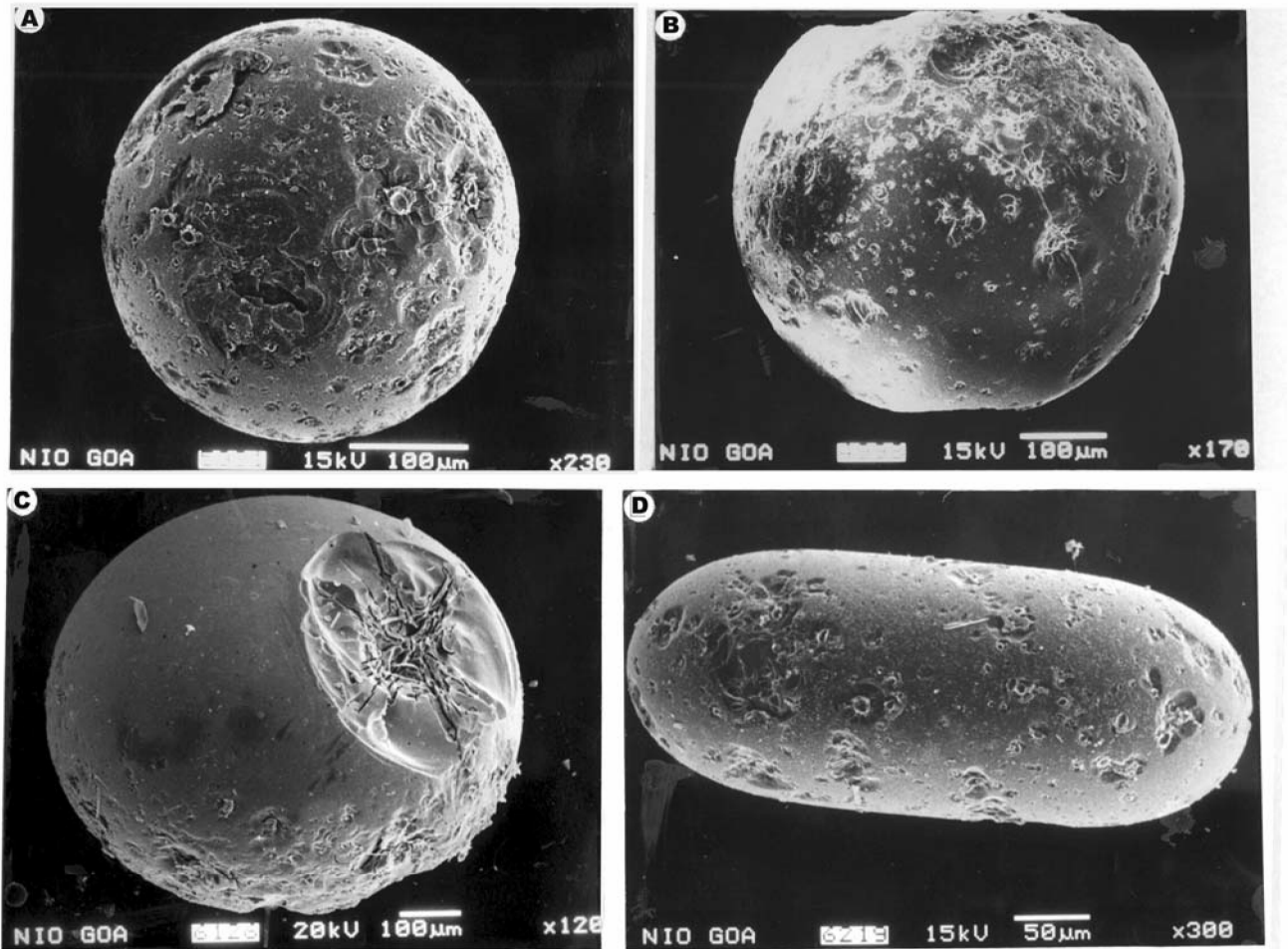
Fig. 2. a) "Small" microtektite with the maximum number of impacts (310 craters) in this study. Two pits are seen to stand out left of center, the spall zone of which is erased by other closeby impacts; b) "medium" microtektite with numerous erosive impacts. A crack seems to run longitudinally along the microtektite; c) a "large" microtektite with a large pitless crater; d) shape does not matter: an elongated microtektite with several erosive impacts.
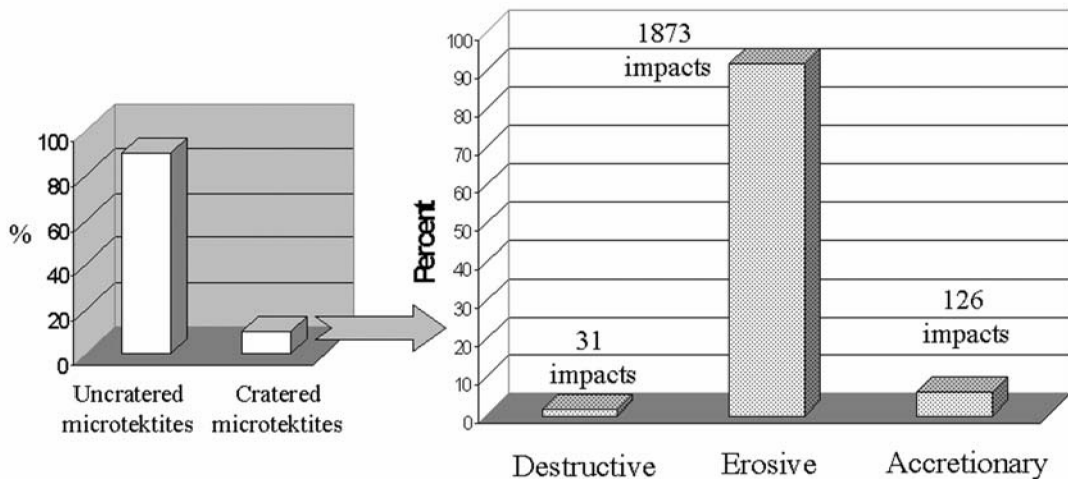

Fig. 3. Percentage of cratered and uncratered microtektites and the types of impacts observed on the cratered microtektites.
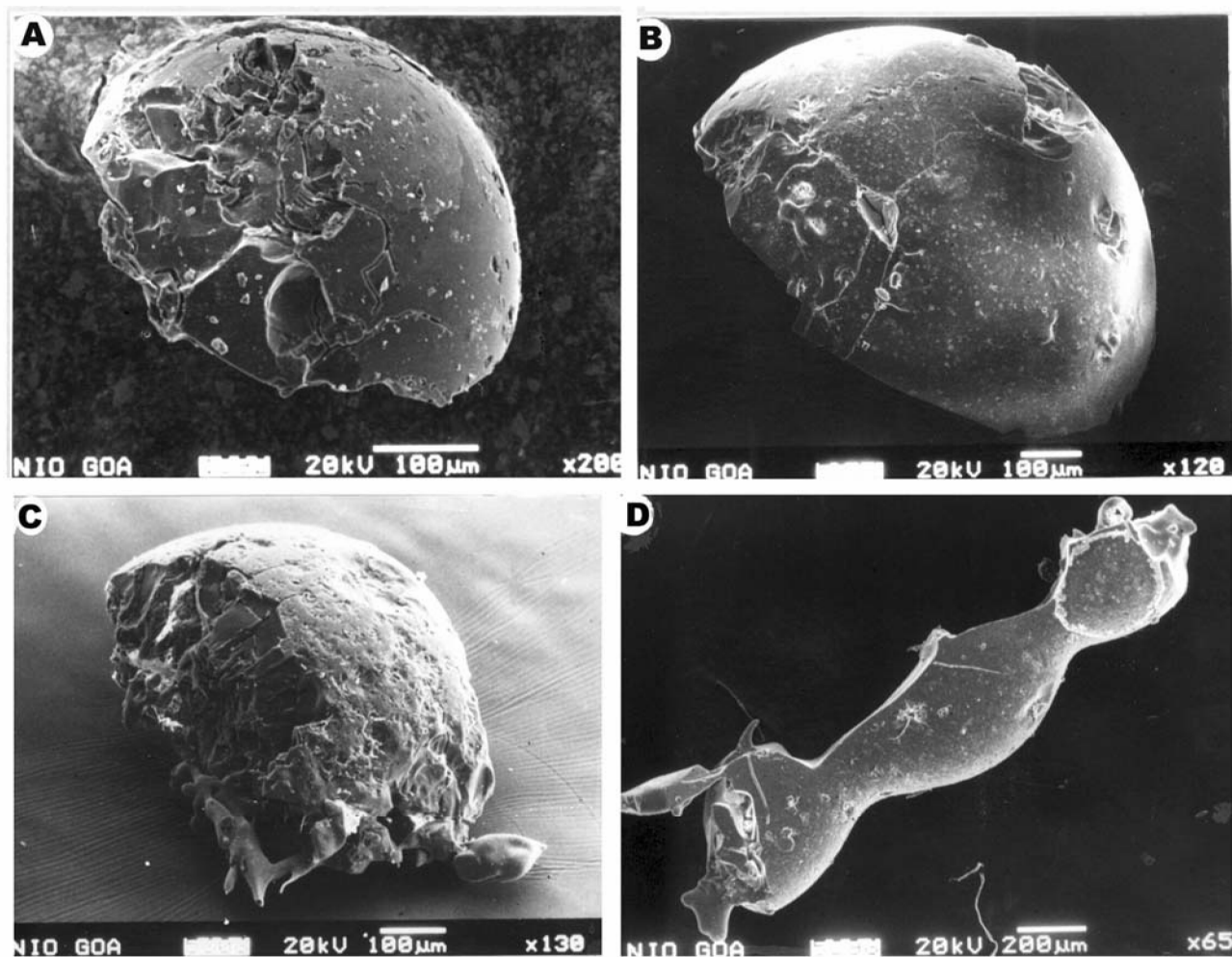
Fig. 4. Fragments: a) a microtektite fragmented into half by collision; b) another fragmented half of a microtektite. Here, several impacts are seen, along with cracks propagating all over the fragment; c) a fragment of a microtektite with extensive cracks propagating from an assumed center, along with some melt; d) a pod-shaped microtektite peeled off the end longitudinally (typical for antipodal regions of destructive collision), while melt at the other end and other craters are also seen.

Erosive Impacts

Erosive impacts dominate the crater population in this study: 92.15% of the total 2030 impacts belong to this category. These range in size from "pit-only" craters, the smallest of which measures 0.3 µm, to the largest 600 µm-sized pitless crater. Different types of erosive impact are observed, and they occur in different size ranges (Fig. 7). As shown in Fig. 1, the number of craters increases with decreasing microtektite size; the relation holds true with respect to the number erosive craters as well. The smaller-sized microtektites have the largest number of erosive craters (and also a larger number of smaller-sized craters), while the larger microtektites possess more accretionery impacts.

Similar to the lunar microimpact population studies, the number density of the crater increases with decreasing crater diameter (Figs. 8 and 9). Further, analogous to the lunar microcrater observations, morphological variations with increasing crater sizes are observed here as well. Their description, given below, follows that of Schneider and Horz (1974).

Pit-Only Craters: Craters which are sub-µm to a few µm in size are "pit-only," i.e., a circular glass-lined pit surrounded by a depressed portion is seen as a positive feature on the host (Fig. 10). Pit-only craters constitute 12.82% of the total impact population (Fig. 11). These types of craters are seen predominantly on the small microtektites (≤450 µm) and a few medium microtektites (450–800 µm) but are absent on large microtektites (>800 µm). When present, they appear in large numbers as close-spaced clusters (e.g., Figs. 10a and 12), indicating sandblasting of the host microtektite.
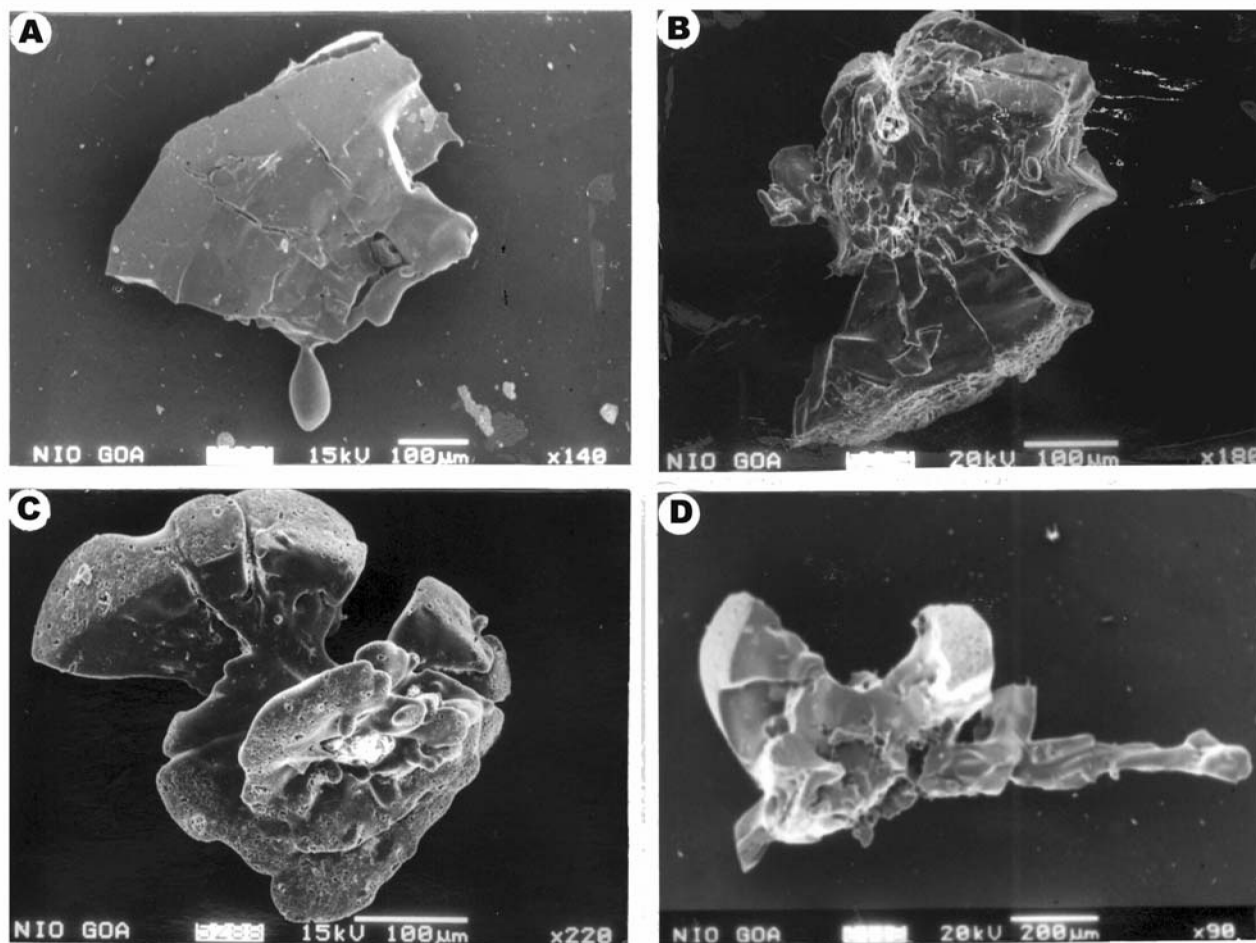
Fig. 5. Crater remnants: a) a remnant of a large crater/microtektite seen with radial cracks and melt; b) a piece of a large crater/microtektite with a central portion partly seen along with radial cracks; c) central melted portions of a crater along with the projectile remnants and radial cracks; d) part of a crater with radial cracks, along with a long melt blob.

Concentric Crack Craters: Concentric cracks are larger than the "pit-only" craters (Fig. 12). The central pit is either cup shaped or a stylus surrounded by concentric cracks. The spallation zone is a moat surrounding the pit, which at times contains radial ridges. These crater types constitute almost 31% of the impacts and are the largest in number densities (Fig. 11). These are found to have a size range of ~1–24 μm (Fig. 7) but mostly less than 10 μm. These are also seen in close-spaced or overlapping clusters. The larger-sized versions of these craters are stylus pit craters and glass-lined pit craters. These crater clusters are seen to be comprised of craters of similar sizes and geometries (Figs. 12c and 12d) or of different sizes, indicating sandblasting of the host by several projectiles and with similar velocities (e.g., Figs. 12a and 12b). Concentric crack craters are confined mostly to the medium to small microtektites and are rarely seen on the large ones.

Glass-Lined Pit Craters: Here, glass-lined pit craters are larger than the concentric cracks and have a central glass-lined pit surrounded by radial and concentric cracks. These are found to occur in size ranges of 9.3–130 μm (Figs. 7 and 13). These constitute 13.51% of the crater population (Fig. 11). These crater types are abundant on the medium and small microtekites and are rarely seen on the large ones. The number of radial cracks seems to vary, especially in relation to the target temperature. In the case of a target or projectile being viscous, the glass-lined pit is in a diffused state without the development of appreciable radial cracks (Fig. 13a). On cooler targets, the central cup is more pronounced, with the triangular radial cracks similar to those typically seen on lunar samples (Figs. 13b and 13d).

Stylus Pit Craters: These craters constitute 17.61% of the total population (Fig. 11). These have a larger size range (5.3–327 μm; Fig. 7) than the glass-lined craters. Stylus pit craters were described first on Apollo 12 rocks by Horz et al. (1971). They were found to have a central raised stylus that becomes more prominent with the spallation of the surrounding
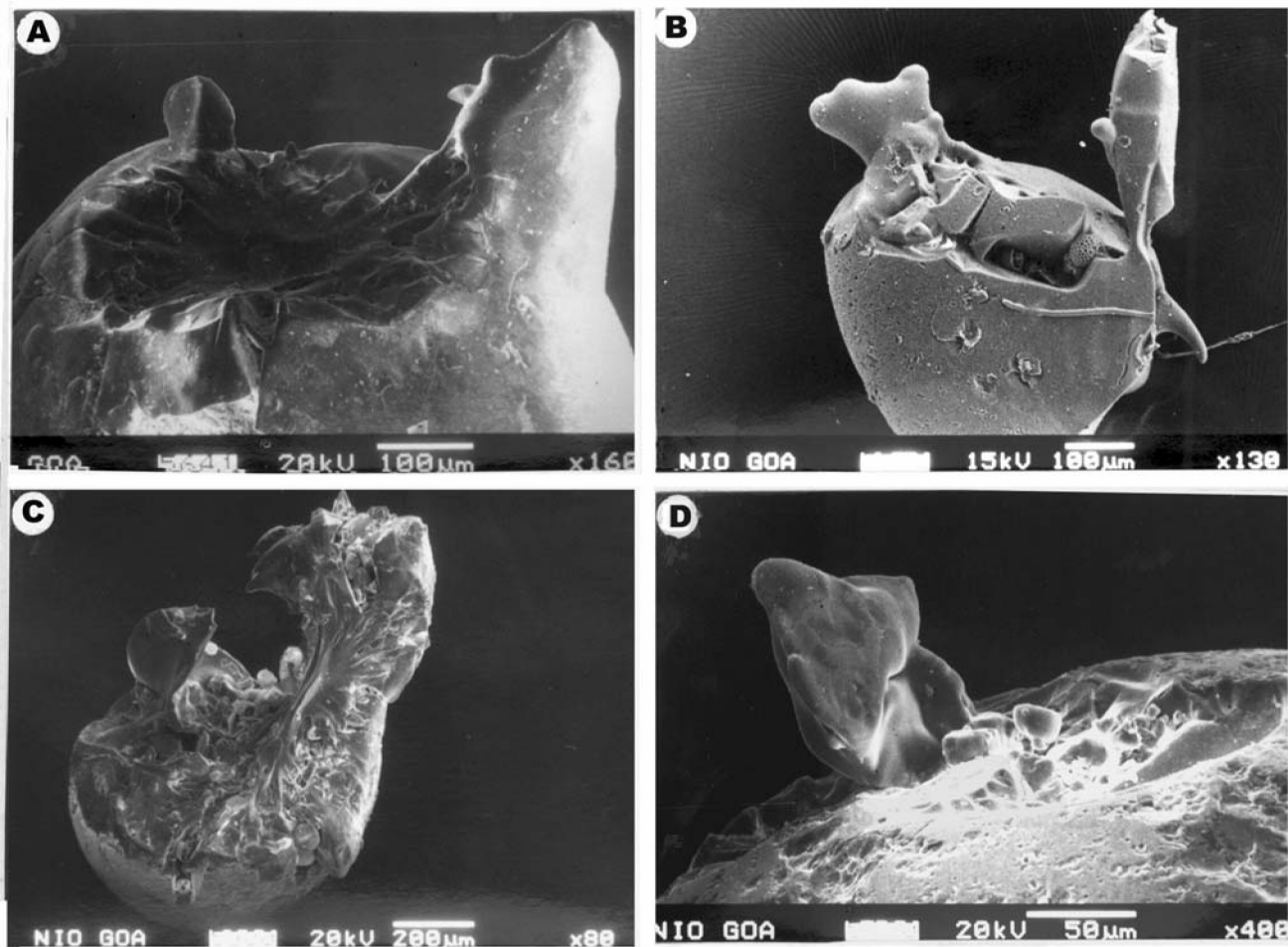
Fig. 6. Protrusions: a) two protrusions are seen: the smaller melt projection on the left and the larger projection to the right, which is a raised portion of the host; b) two protrusions are also seen here. The melt projection on the left is a molten portion of the host, and on the right, a portion of the target that is angular is broken and raised; c) massive collision has pulled out a portion of the molten host. An overturned flap is seen, indicating the direction of the impact. Flow schlieren are also seen. A portion of the host that has been bent backwards and raised is discernible; d) a solid, low-velocity fragment impacted a still viscous host.
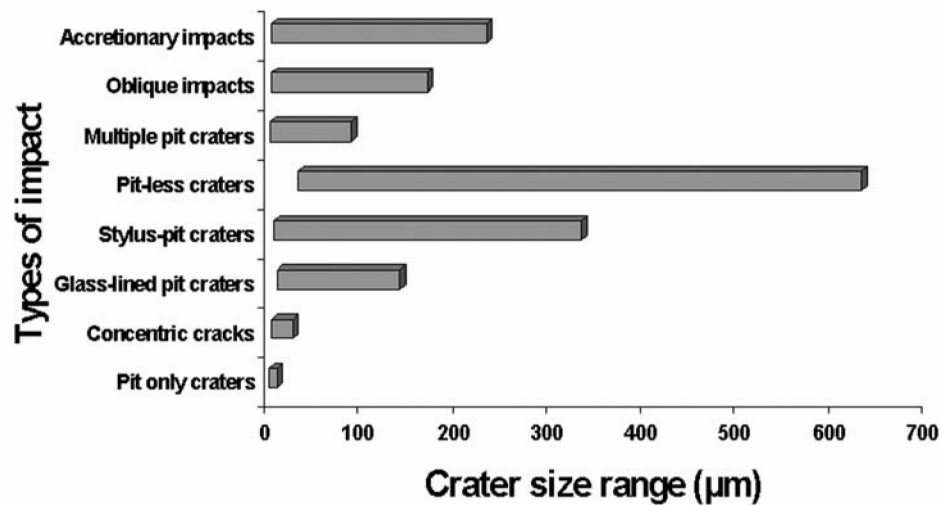

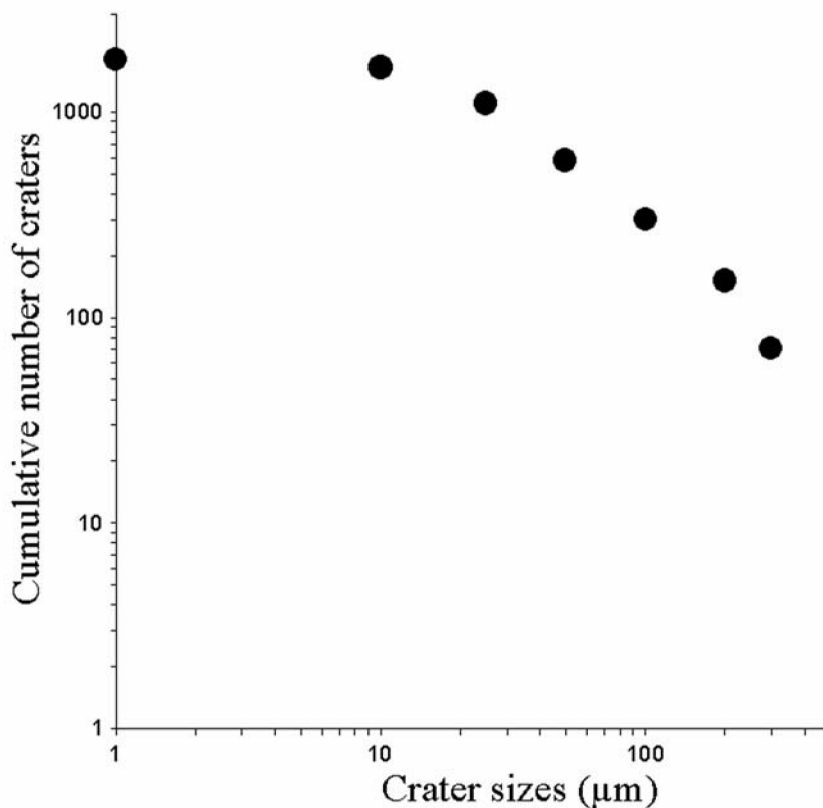Fig. 7. Size ranges of the different types of craters.

Fig. 8. Absolute number of craters counted on all the samples.

material. Here, the stylus pit craters are found on all 3 size classes (small, medium, and large) of impacted microtektites but are present in larger numbers on the medium and smaller size classes. The central stylus shape is angular or hummocky (Figs. 12a and 14a) where the radial cracks are fewer and the craters are shallow. The development of the stylus on these craters seems to be due to elastic rebound on a heated, viscous target. With increasing hardening of the target, the plastic flowage disappears and the triangular radial cracks and concentric cracks are seen (Figs. 14b and 14c). The central stylus seems to take the shape of a raised platform in these cases, or an incipient shallow cup is seen. In a few extreme cases, the radial cracks, ridges, and also a part of the stylus are removed by other impacts on the microtektite (Fig. 14d).

Pitless Craters: These are the dominant erosive impact features on large microtektites. Pitless craters are found in size ranges of 31–600 μm (Figs. 7 and 15) and many craters are >200 μm in diameter. The percentage of pitless craters is 11.26% of the crater population (Fig. 11). They are invariably shallow and have a central flat portion surrounded by a few radial and concentric cracks (Fig. 15). Flowage can be seen on a majority of the pitless craters (Figs. 15a and 15c). In general, pitless craters have fewer cracks than glass-lined or stylus pit craters; and the typical triangular cracks, seen on the latter, are also rare. Further, with hardening of the targets and with higher impact energies, the pitless craters seem to grade into stylus pit craters (Figs. 15c and 15d).

Multiple-Pit Craters: Overlapping craters that have a common spall zone (Fig. 16) comprise 5.63% of the total erosive crater population (Fig. 11). These craters have a size range around 1.4 μm where 2 submicron projectiles have impacted the same spot on the host, and the largest multiple-pit crater measures ~80 μm. The sizes refer to the outermost extent of the spall zone common to both of the impacts. These are either double-pit craters, where 2 projectiles impact the same spot, or multiple-pit craters, where more than 2 projectiles impact in a cluster. Here, the projectiles sizes are similar and appear to have impacted the host together at similar velocities (Fig. 16). With increasing space between the impact spots, the development of individual glass-lined pits is seen. No pitless craters are seen either in this category or stylus pit craters.

Incipient Craters: Incipient craters are erosive impacts but of a lower impact velocity, resulting in incomplete craters. Only a central pit and very few radial cracks are observed (Fig. 17a), or in the oblique category, an elongated pit (due to an oblique impact and half a radial crack downrange) is observed
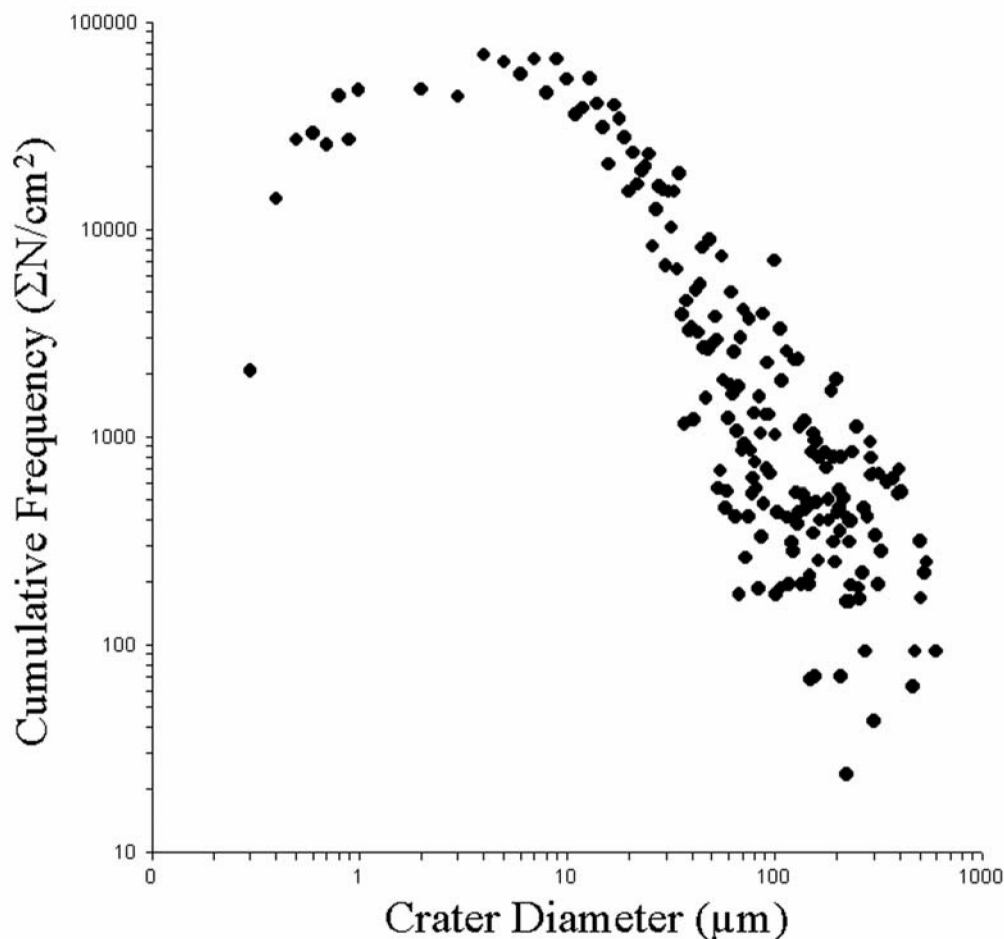
Fig. 9. Cumulative crater number densities versus crater diameter.

(Figs. 17b and 17c). This type of crater is rare and implies very low impact energies.

Oblique Impacts: Oblique impacts form 8.15% of the crater population (Fig. 11). They are found in the size range of 3.9–210 µm (Fig. 7). The size given here is the actual length of the longer dimension of the craters. Logically, most impacts on microtektites have to be oblique given their spherical shapes; however, a majority of impacts are centro-symmetric. Gault and Wedekind's (1978) experiments have shown circular craters up to an incident angle of 30°. Here, impacts identified as being due to oblique incidences show a varying departure from circularity (Fig. 18). The least oblique impact shows an oval crater with a pit on one side and radial and concentric cracks downrange (Fig. 18a). With increasing obliquity, the craters become elongated grooves with flow on either side and with downrange deepening and widening of the grooves (Fig. 18c). Where the projectiles are in a diffuse state, the grooves are shallow with fingers of melt downrange (Fig. 18d). Extreme oblique incidence causes an elongated furrow that is very shallow. The projectile imparts a glancing

blow and passes through (ricochets?), possibly onto other particles that are in flight. If the impact energy is high, then it would impart spin to the target, making it a target for many more oblique impacts. Target shape also seems to play an important role—a disk-shaped microtektite has 27 oblique impacts on one side because the host presents itself as a flat plate to the projectiles.

Accretionery Impacts

The crater population in this study includes 6.21% that are due to accretionery, low-velocity impacts (Fig. 19). A spall zone is generally absent, and a quasi-plastic target is required for the accretionery impacts to register. Accretionery impacts range from projectiles that are gently welded to the host (Fig. 19a) to projectiles that are disrupted, half-buried, or flattened upon impact, depending on the plasticity of the target or projectile. Some of the larger impacts in this category are seen as pancakes with moats around them (Fig. 19c). Spatter is also seen on some microtektites as discrete lumps or as small, fluffy particles sprayed over the surface (Fig. 19b). Scratch marks and grooves are also seen
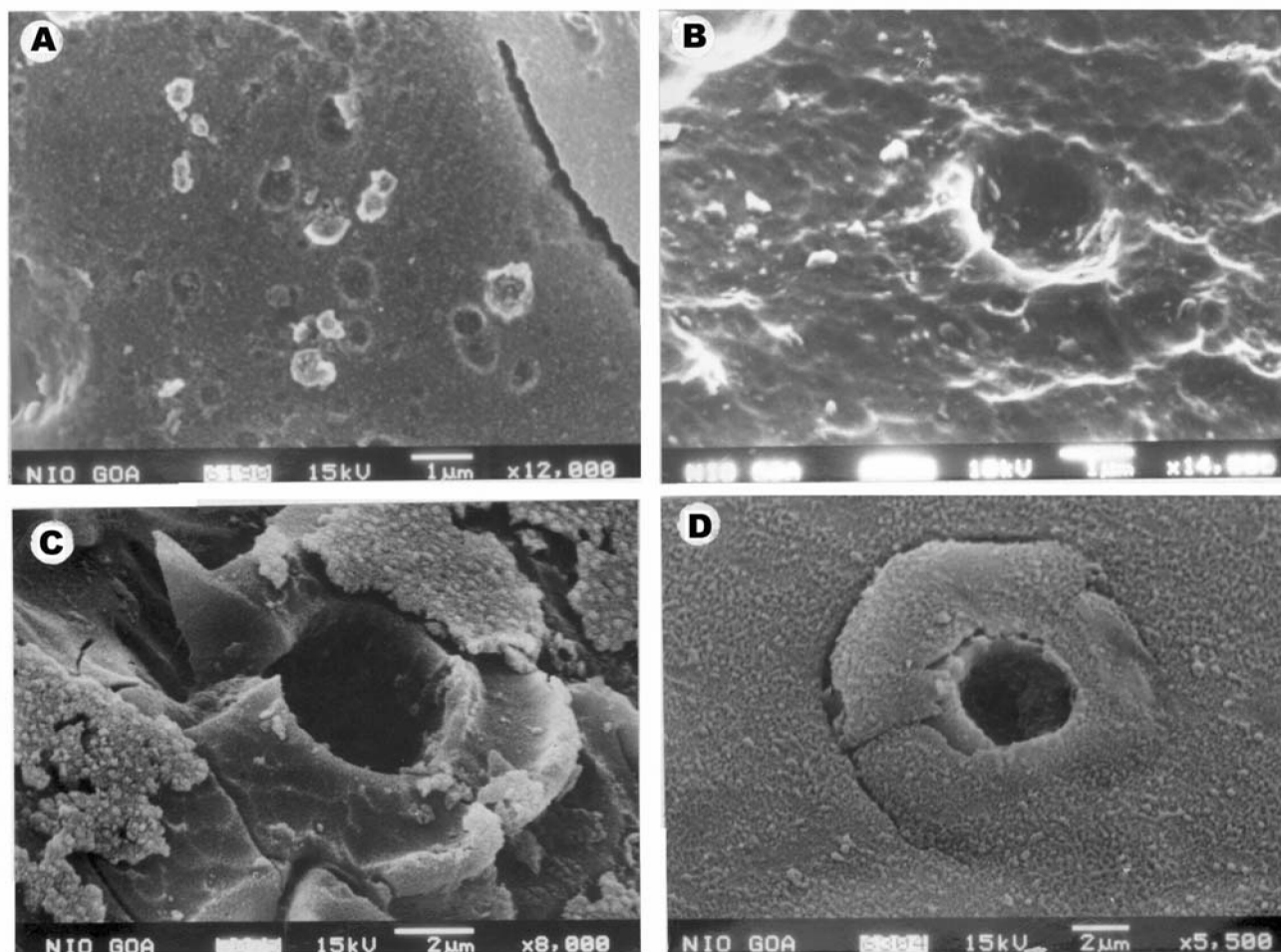
Fig. 10. Small craters: a) small doughnut-shaped craters with annular rings as crater rims; b) a bowl-shaped crater with flow rims; c) a pit-only crater with a raised rim and flow; d) a pit-only crater with incipient development of concentric cracks.

(Fig. 19d), which indicates low-velocity collisions on lunar spherules (Hartung et al. 1972).

DISCUSSION

In our earlier study (Prasad and Sudhakar 1998), only those impact features on microtektites that showed melt or accretionery phenomena were categorized as being due to impact. This approach left out many others that had hypervelocity impact features, especially the smaller-sized microtektites, which, as observed here, have the largest number of impacts, mainly of the erosive type. The smallest impacted microtektite reported earlier had a diameter of 590 μm, while in this study, 180 μm is the diameter of the smallest impacted microtektite. Furthermore, the smallest impact feature identified in our earlier studies was an accretionery feature of 35 μm and the smaller craters, which occur in large numbers, were not identified at all. In the present detailed study, several microtektites, which would show up as etched in the binocular microscope, are seen to be clusters of impacts in the SEM. Consequently, more than an order of magnitude additional craters are identified now. Further, we now observe that the microtektites with the largest diameters have the least number of craters and that the crater density increases with decreasing microtektite size (Fig. 1). Also, fragments were not considered earlier, although they should form an important component of the impact process, indicating the destructive capabilities of inflight collisions.

All of the observed features are comparable with lunar microimpacts. Similar to the crater remnants, individual "pits" of craters have been reported from the lunar fines, which were suggested to be dislodged from pit craters (Schneider and Horz 1974). Craters with positive rims and fluid flow similar to the pit-only craters have been described by McDonnell et al. (1975). Further, concentric cracks comprise 0 to 17% of the total of 6000 craters on 12 rocks of Apollo 17 (Schneider and Horz 1974) and have been found on Luna 16 spherules as well (Hartung et al. 1972). Concentric cracks are suggested to be transitional between the pit-only craters and those with pits and radial and concentric cracks. Their transitional nature can
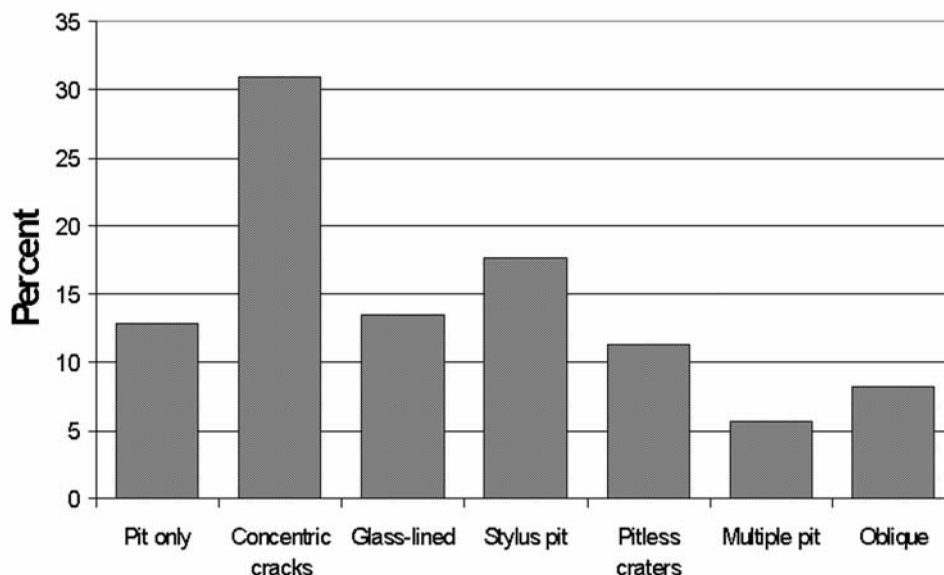
Fig. 11. Types of erosive impacts.

be seen when observed in clusters of different sized craters (e.g., Fig. 12b). The glass-lined pit craters are the most common types of microcraters on all lunar materials and form the crux of the lunar microcrater interpretations (e.g., Horz et al. 1971; Schneider and Horz 1974; Neukum et al. 1973). Horz et al. (1971) illustrated styli of different geometries for stylus pits, many of which are seen here as well (Fig. 14). Some of the stylus pit craters shown here are similar to the craters generated by Carter and McKay (1971) as secondary impacts on a target heated to 700°C (e.g., Fig. 12a). They also observed protrusions.

On lunar spherules, the pictures presented by Carter and MacGregor (1970) and McKay et al. (1970) show pitless craters to be larger than the pit craters, and a secondary origin has been proposed for all the craters. Among a crater population study of 10,000 craters on Apollo 16 rocks, Schneider et al. (1973) found that the pitless craters vary from <5–20% of the total crater population. Schneider and Horz (1974) found that the pitless crater abundance was higher on surfaces of low crater density (as in this study). In view of this, they did not eliminate the possibility of a secondary origin due to collision during the rock's ballistic trajectory to the eventual site of recovery. Further, in contrast to the data presented here, Schneider and Horz's (1974) data did not show any size differentiation between the pit craters and the pitless craters. Multiple-pit craters have also been seen on lunar rocks. However, the craters observed here are different from those presented by Horz et al. (1975) in which a diffuse projectile seemed to have impacted lunar glass surface 15286. Some of the craters seen here are close to the multiple-pit crater produced in the lab by an aggregate of SiO$_2$ glass spheres into soda lime glass (Horz et al. 1975); however, the development of a common spall zone is seen here.

Experiments generating oblique impacts (Gault and Wedekind 1978) showed downrange grooves on noncohesive targets at impact angles <10° (Gault and Wedekind 1978). Here, however, the grooves were seen to be narrowing downrange in contrast to widening. Accretionery impacts were observed on lunar rocks (Horz et al. 1971) and spherules as well (Hartung et al. 1972). They seem to be the results of low-velocity collisions on a target that was hot and viscous, as can be observed by gentle welding of projectiles accompanied by flow, an absence of spall zones, and the presence of scratch marks (Fig. 19).

Projectile Energies

Considering the range of impacts from low velocity accretionery features through all categories of erosive features and, finally, the destructive impacts, a vast range of impact energies are involved. Assigning accurate impact velocities is difficult because the targets are in various stages of cooling and solidification. However, based on their resemblance to features produced during simulation experiments, the following explanations are presented.

Obviously, accretionery impacts are gently deposited onto targets that are invariably hot, as can be seen by the plasticity of the targets (Fig. 19). However, some level of comparison with simulation experiments can be made with respect to the erosive impacts. For the generation of the pit-only craters of few microns in size on glass, a projectile velocity in the range of about 3 km/s is required (Vedder and Mandeville 1974). However, for craters a few µm in size but with appreciable spallation zones and radial and concentric cracks, higher velocities (5–14 km/s) are required (Vedder and Mandeville 1974).
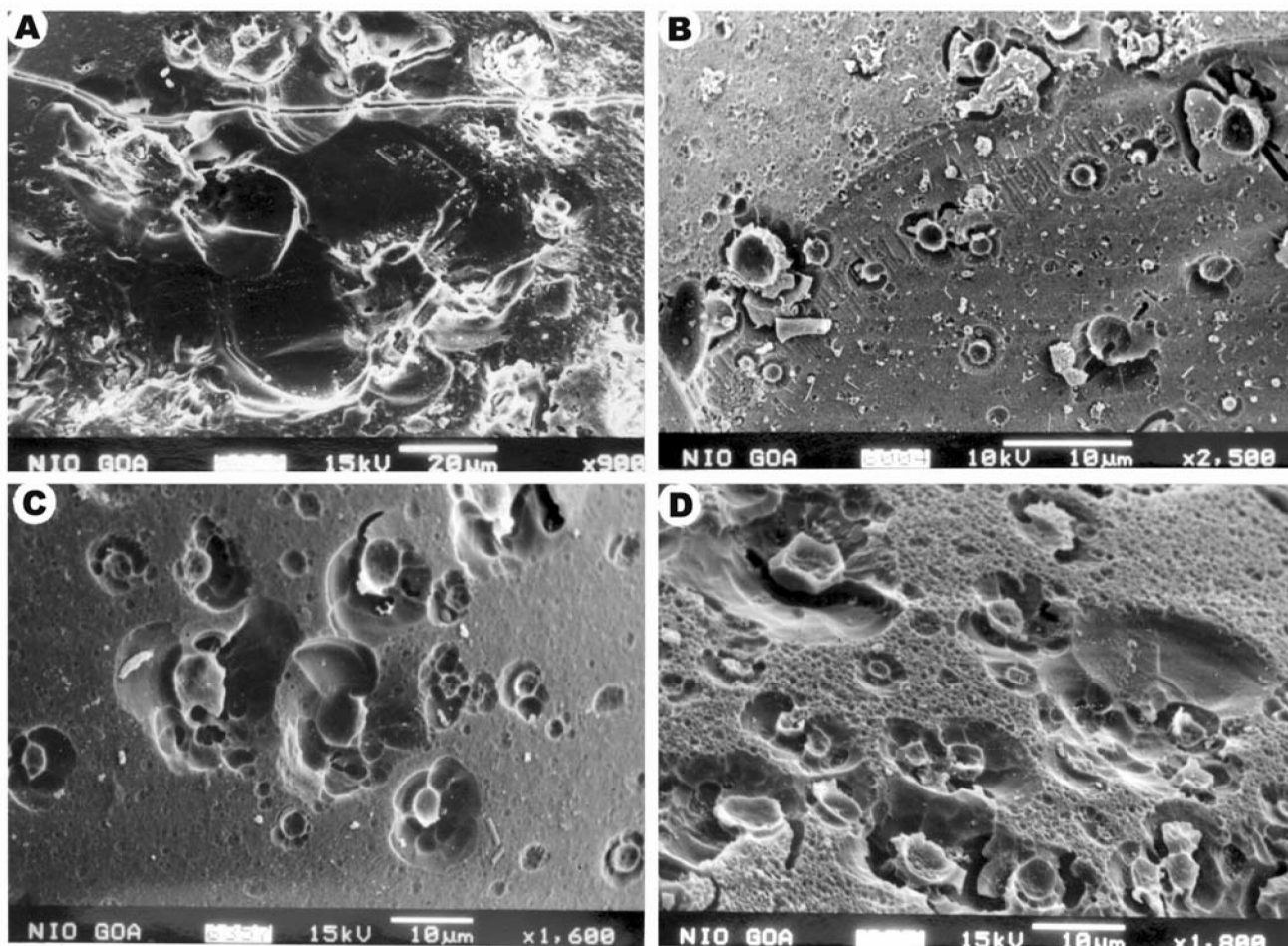
Fig. 12. Sandblasted microtektites: a) cluster of craters of different sizes. The larger craters seem to develop stylus pits, the smaller ones are pit-only or concentric cracks; b) a relatively large portion of a microtektite. Many craters are located in the spall zone of the large crater seen in Plate 1A. Craters ranging from pit-only through concentric cracks and larger glass-lined pit craters all co-exist in the same area; c) several close-spaced multiple impacts; d) a close-up of a small cluster of craters. The central stylus is surrounded by radial ridges and concentric cracks and other smaller concentric crack-type craters are seen.

Glass-lined pits have been commonly generated during several simulation experiments (e.g., Vedder 1971; Bloch et al. 1971; Vedder and Mandeville 1974; Fechtig et al. 1978; Horz et al. 1975). The above experiments have established the threshold velocity conditions for generating craters of this geometry on glass—the minimum impact velocity required is 3.5 km/s (Vedder 1971; Vedder and Mandeville 1974). Neukum et al. (1972) simulated stylus pit craters at a primary impact velocity of >3 km/s. Some of the craters presented here have a resemblance to those simulated at 12 km/s on glass by Vedder and Mandeville (1974) (e.g., Fig. 13d). Pinning down the velocity for the oblique impacts is difficult. However, some of the craters resulting from higher incidences, which also show a pit as well as radial cracks (e.g., Fig. 18a), could have had impact velocities close to 3 km/s. Vedder's (1971) data shows a crater on glass generated at 30° and 8.2 km/s velocity that has a triangular groove that broadens downrange. Similar craters at lower

velocities have been shown by Horz et al. (1975). The oblique impacts shown here have similarities to both types. However, they differ with the low angle (<15°) impacts generated by Gault and Wedekind (1978) in having downrange widening and deepening of the grooves; they used a non-cohesive target, in contrast to the host used in this study.

All of the above simulation experiments were carried out on relatively cool targets at room temperatures. However, Schneider et al. (1990) generated craters on glass with extensive cracks at an impact velocity of 3.69 km/s on a target heated to 70°C. Carter and McKay (1971) carried out simulation with incremental heating of the targets. Both of the above investigative groups observed that the target strength is reduced considerably at elevated temperatures. The target temperatures here are unknown. Several hosts show evidence of being hot when impacted (e.g., protrusions and flow). Thus, pin-pointing the velocity required for generating glass-lined pit craters on tektites may be difficult because a majority
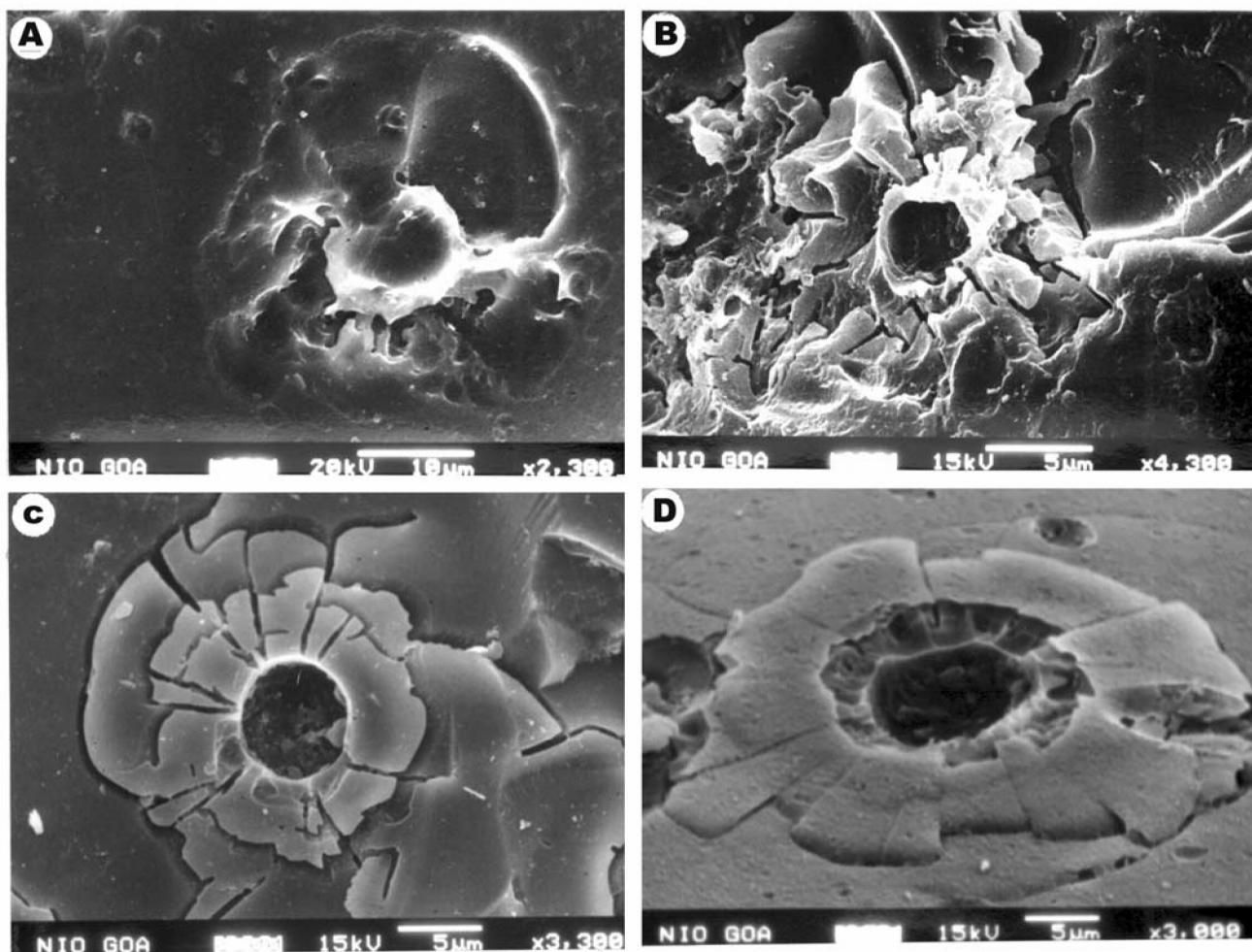
Fig. 13. Glass-lined pit craters: a) a diffuse central glass-lined cup being formed with radial ridges and spall zone (indicating lower velocities) on quasi-brittle targets; b) a glass-lined pit crater with prominent central cup and well-defined radial cracks; c) a glass-lined pit crater which appears flat. A nearby impact has erased the positive feature of this crater; d) a central glass-lined pit crater along with well-defined radial cracks that bears a resemblance with that simulated at 12 km/s impact velocity by Vedder and Mandeville (1974).

of them may not have cooled completely during the time of impact. Further, the large-sized pitless craters on some microtektites have spall diameters that are close to the diameter of the host itself, suggesting that they are low-velocity impacts. A higher impact velocity would have fragmented the host. Clearly, however, sufficient relative velocities are generated within the entrained ejecta to result in glass-lined pit craters and stylus pit craters.

Overall, the projectile energies, which basically represent the relative velocities between the entrained ejecta of the impact that produced the Australasian tektites, have a wide range. Two aspects seem significant here:

1. Spherule formation is an important part of impact cratering, and the sizes of these condensed droplets form an essential parameter in estimating impactor size and velocity (Melosh and Vickery 1991).
2. While it has been established earlier that the impacts seen on microtektites are due to interparticle collisions

within the ejecta plume (Prasad and Sudhakar 1996, 1998), the specific timing of the collisions during flight from Southeast Asia to the eventual place of deposition (Central Indian Ocean) is also discussed here.

Projectile Sizes

About 1 billion tons of ejecta have been estimated to have been generated by the Australasian impact event, and the average microtektite size is suggested to be ~200 µm (Glass et al. 1979). Subsequent calculations (Schmidt et al. 1993) estimated the mass of the Australasian tektite material to be much larger. The microtektite abundance (number of microtektites/cm^2) seems to increase with decreasing microtektite diameter. We observe that the abundance of microtektites in the 125–250 µm size range is 1.5–2 times that of the >250 µm sizes (Table 1). Interestingly, Burns (1990) studied microtektites in the 63–125 µm size fractions and
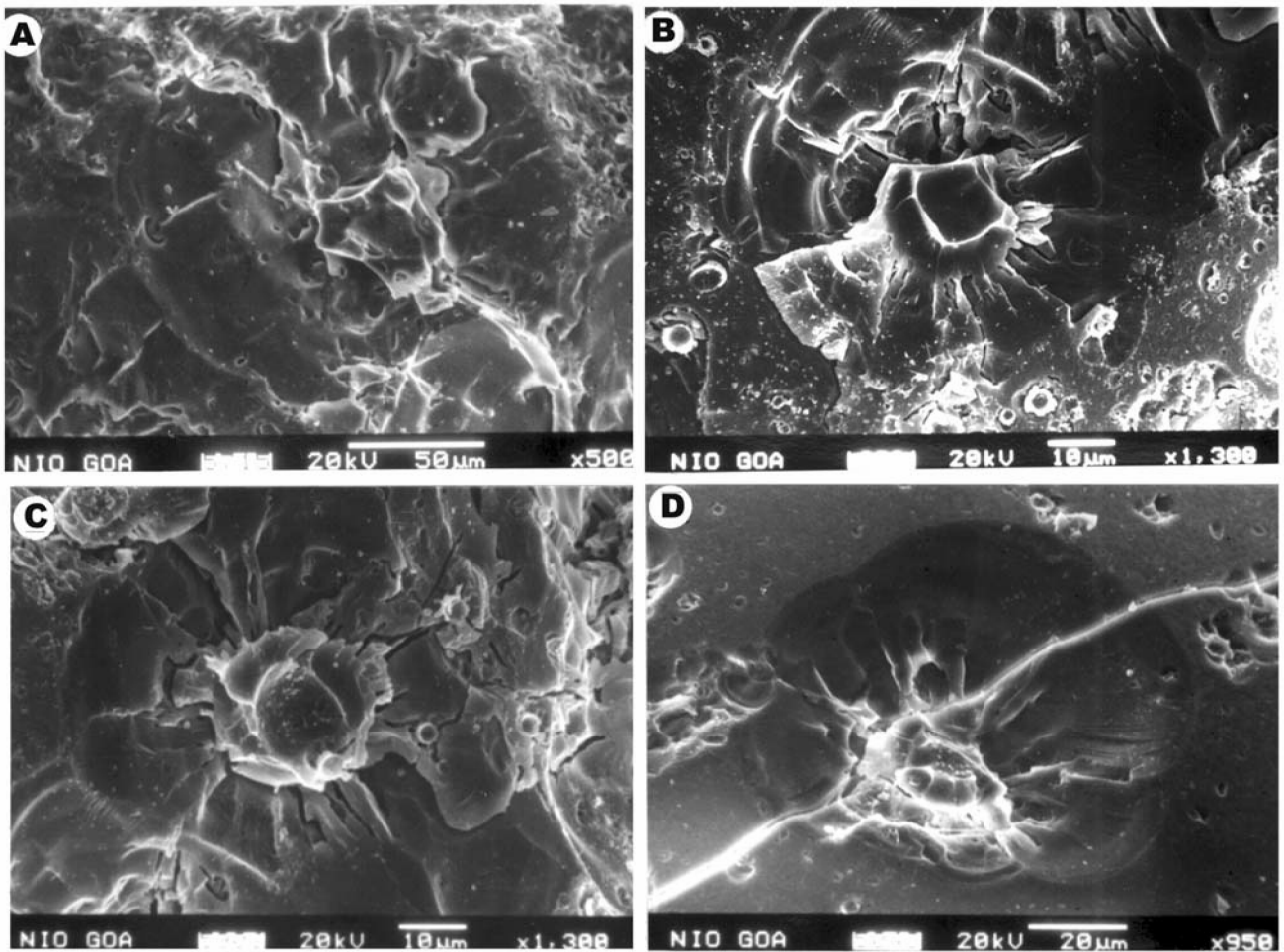
Fig. 14. Stylus pit craters: a) an angular, raised stylus at the center along with melt flow, radial cracks seem to be almost non-existent; b) a central raised platform of a stylus with triangular radial cracks seen in the unspalled region; c) a central raised cup stylus with surrounding radial ridges seen due to the spallation of radial cracks. Smaller craters seen in the spallation zone on the right; d) a portion of a stylus remains in the crater as well as a few radial ridges. The radial cracks, etc. seem to have been spalled. A crack runs through the crater. Other smaller craters are seen in the vicinity.

found their abundance to be twice that of those >125 µm. Microtektites with sizes lower than these are very difficult to isolate from the deep sea sediments. The abundances in the Central Indian Ocean are found to be up to 120/cm^2 for microtektites of >125 µm size (Glass and Wu 1993). To relate the crater diameters to droplet sizes, several simulation experiments are available. For example, Bloch et al. (1971) demonstrated the projectile size to be one half of the pit size at 20 km/s impact velocity. In this study, pit-only and concentric cracks constitute about 44% of the erosive impacts. Their pit sizes are either sub-µm or <~5 µm. Here, since the temperature of the host when it was impacted is unknown, we can assume safely that the projectile size should be less than the pit size. Therefore, a majority of the projectiles here are either sub-µm or a few µm in size. Clearly, while a large mass of the ejecta is concentrated in the bigger microtektites/tektites, the number density of smaller particles that form

projectiles in the micron and submicron ranges also appears substantial. These data have significance in understanding tektite-producing impacts. Because the material melting or condensing from the vapor plume of an impact will tend to condense as small spheres the sizes of which are limited by the surface tension's ability to overcome aerodynamic stress (Melosh and Vickery 1991), the total fine ejecta volume is expected to be sensitive to impact velocity (Lorenz 2000).

Timing of Impacts

The small microtektites, which have the largest number of erosive craters, seem to have been caught in a dense swarm of fast-moving projectiles in the µm and sub-µm sizes. That large microtektites have fewer craters and that those present require lower impact velocities is, indeed, surprising (e.g., accretionery impacts and pitless craters). Based on the
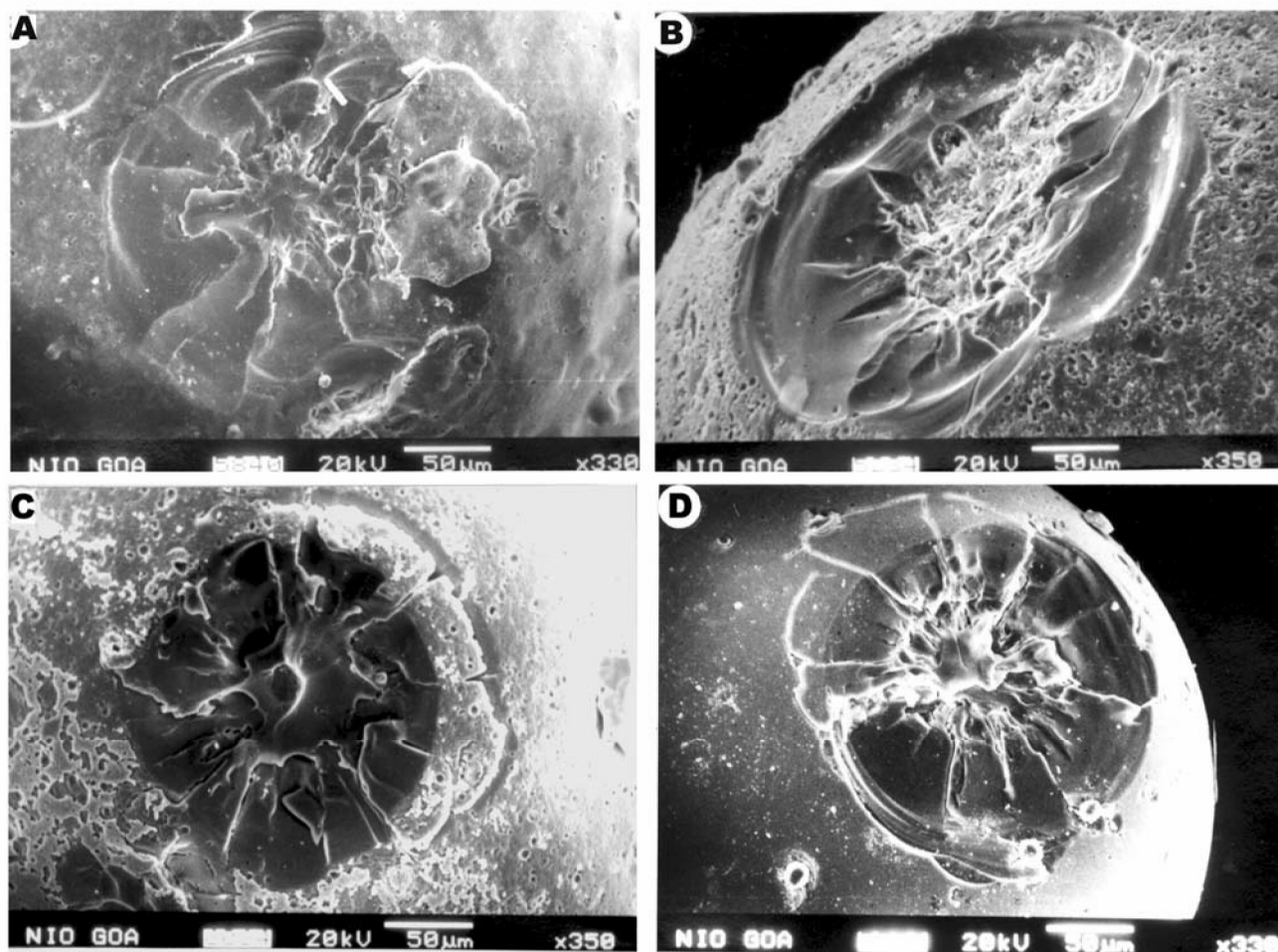
Fig. 15. Pitless craters: a) shallow pitless crater with a molten portion in the center and a few diffuse triangular cracks; b) a central portion with a diffuse flattened portion and but no triangular radial cracks. A spallation zone, however, is developed; c) an almost flat crater with a central raised molten portion and radial triangular crack development, with concentric cracks as well; d) a crater on a more hard target than (c) above, with a central raised molten portion, surrounded by melt and triangular radial and concentric crack systems. Other smaller glass-lined pit craters are also seen in the vicinity.

existing models on impacts, Prasad and Sudhakar (1998) suggested that differential velocities between the ejecta of different sizes leads to collisions, and further, multiple sequential impacts in the dense swarm add to the number of impacts on each microtektite. However, fewer numbers of impacts on large microtektites and the presence of more violent impacts registered exclusively on small microtektites is puzzling, especially considering that ejecta of vastly different sizes are recovered from the same sampling spot having an area of a few cm^2.

Impact modeling studies suggest that a tektite-producing impact throws up large volumes of material, including larger-sized solid rocks in the vicinity of the crater, as seen in the Ries Crater (Horz et al. 1983), and the size of the ejecta decreases radially away from the crater, as clearly seen in the Australasian strewn field. Large volumes of vapor and ejecta are thrown up, accompanied by the removal of atmosphere, and

these then interact with each other (Vickery 1986; Melosh 1989). The above models present plausible scenarios for interparticle collisions within the ejecta. Apparently, although both small and large microtektites had similar trajectories (they were recovered from the same core), the small microtektites should take relatively little time to cool and, therefore, can withstand high-velocity impacts within the threshold values given by Gault and Wedekind (1969). On the other hand, the large microtektites that cool slower can only withstand low-energy impacts. This conforms with the data presented here (Fig. 1). Therefore, the large microtektites solidified at a time (and place) when the "projectile" density was lower.

Further, theoretical studies suggest, in the presence of atmosphere, subsequent winnowing of the plume takes place at distal regions from the impact site (Schultz and Gault 1985) before they are finally deposited. This model supports the possibility for collisions some distance away from the crater.
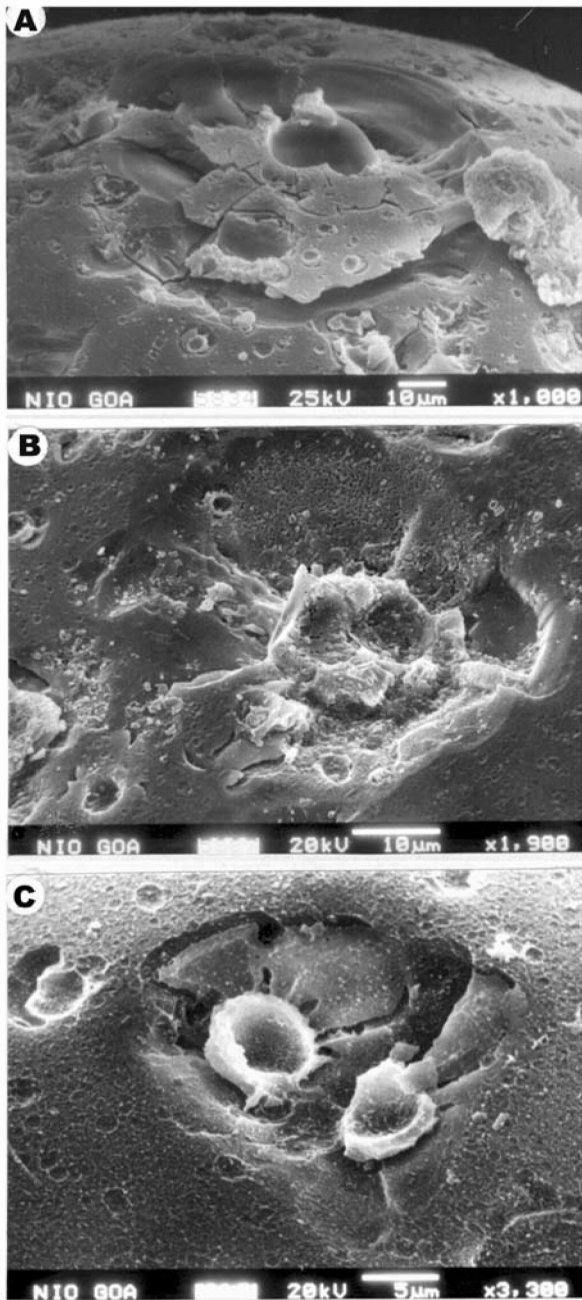
Fig. 16. Multiple-pit craters: a) two projectiles impacting simultaneously. A heart-shaped central pit with radial and concentric cracks common to both the impacts is seen; b) two projectiles impacting with less overlap than in (a) above. A common spall zone is seen; c) two glass-lined pit craters generated by the simultaneous impact of 2 projectiles, with slightly farther spacing than on (a) and (b) above. Triangular, radial cracks, and common concentric cracks for both are seen.

The locations of all 4 cores are at approximate distances of ~4000 km from Indochina (the most plausible impact site for Australasian tektites). Interestingly, an ablated tektite was recovered from one of the core locations (AAS 4/6) (Prasad
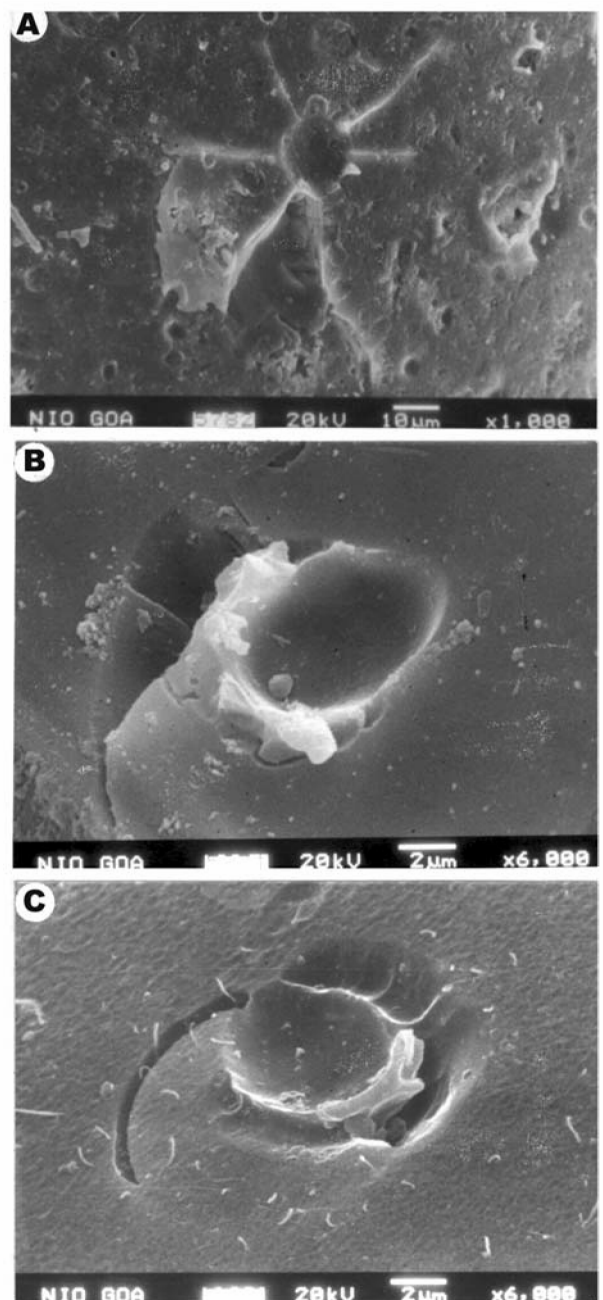

Fig. 17. Incipient craters: a) a central shallow pit with radial cracks and part spallation; b) an oblique impact with a triangular cup and a radial crack; c) another shallow cup with part spallation zone and one radial crack.

and Rao 1990). The ablated anterior side of this tektite contains a high-velocity impact crater (Glass et al. 1996). Evidently, the collision producing this crater took place at the end phase of ablation, a few thousand km from the Australasian tektite source region.

Further, fragments as seen here (Figs. 4 and 5) are definitive indicators of catastrophic collisions within the
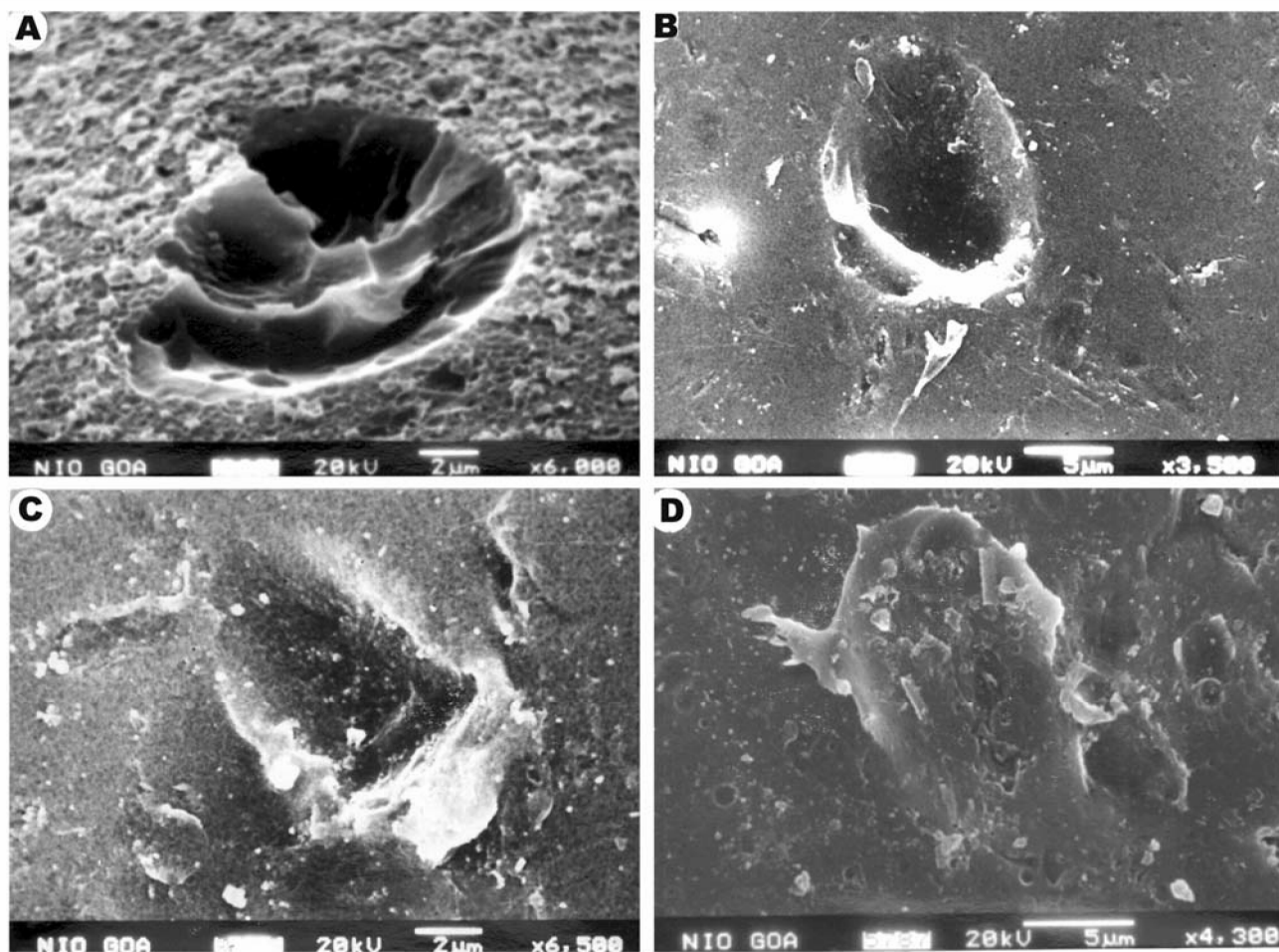
Fig. 18. Oblique impacts in a sequence of increasing obliquity: a) a high-angle oblique impact. The development of a pit is seen; b) a deep high-angle oblique impact; c) steeper angle of impact than the previous ones with downrange widening of the groove and flow along the groove; d) molten flow downrange with fingers of melt sticking out, suggesting the involvement of a molten projectile impacting at a very steep angle.

plume. A maximum of 41% of fragments are shown by Glass et al. (1997) in the proximity of Indochina. Their data show a decrease in fragment percentage with increasing distance from the impact site in Indochina and at the locations of the samples in this study (a distance of about 4000 km from the putative source region in Indochina [Glass and Pizzuto 1994]); the percentage of fragments varied from 0–13%. The cause for fragmentation as suggested by Glass et al. (1997) is the break up of tektite material due to thermal stress upon landing on the ocean surface. Apparently, this distance from the source region, catastrophic collisions within the ejecta plume can also contribute to fragment population.

Microimpacts in Other Strewn Fields?

Impact microcratering has been reported only on the Australasian impact ejecta (Prasad and Sudhakar 1996; 1998; Glass et al. 1996) among the terrestrial materials. Interestingly, Margolis et al. (1971) found impact splashes

beneath the flanges of australites. Further, fused microtektites have been reported on Ivory Coast and North American microtektites (Glass 1974) where, clearly, the fusion of these microtektites has taken place during their flight to the eventual place of deposition. Apparently, the microimpact phenomena seems to be occurring in all tektite-producing impacts. It would be interesting to know whether such interparticle collisions are restricted only to tektite-producing impacts in which an oblique trajectory of the impactor, sedimentary substrate, melt production, and removal of atmosphere are the primary requisites.

Lunar Microcratering

The impacts seen here are similar in many ways to those observed on lunar rocks, breccia, and glass spherules. Crater morphology variation with size (Hartung and Horz 1972; Schneider and Horz 1974; Morrison et al. 1973; Horz et al. 1975; and others) is as seen here. The entire range of crater
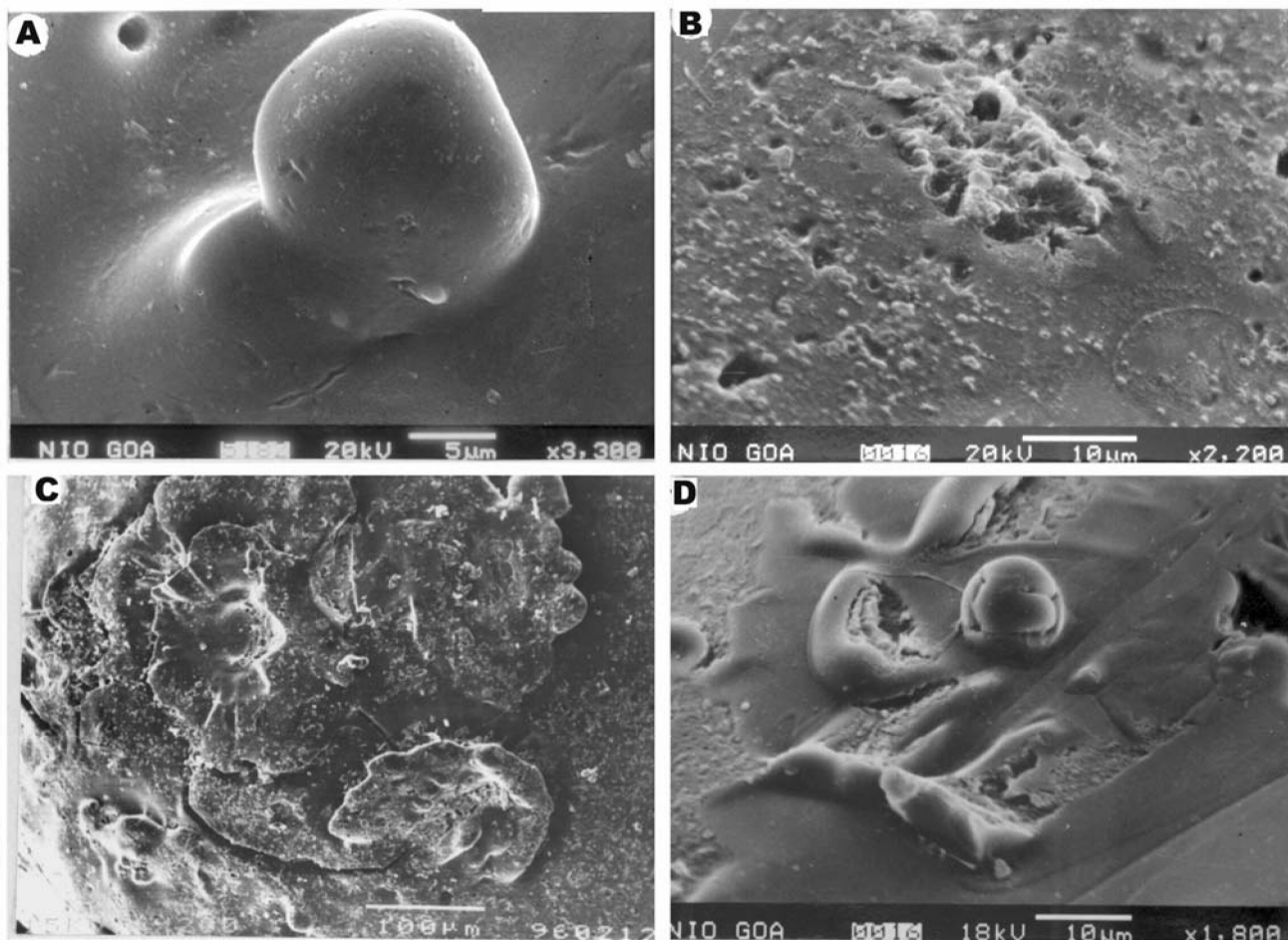
Fig. 19. Accretionery impacts: a) an oval projectile gently perched on a microtektite; b) spray of material on a microtektite surface; c) low-velocity impact similar to a pancake; d) scratch marks and flow on a microtektite surface.

geometry (pit craters, stylus pit craters, concentric cracks, sub-μm craters, oblique impacts, and low-velocity accretionary impacts) is similar to that of the lunar materials. Further, the high number density of small craters evidenced here (Figs. 4 and 5) has been seen typically on all lunar microcrater population studies (Horz et al. 1975; Morrison and Zinner 1977; Grun et al. l985; and others). Schneider et al. (1973) found exceptionally large numbers of craters in the micron and sub-micron ranges on Apollo 15, 16, and Luna samples, leading them to suggest a bimodal size distribution of interplanetary dust. However, a need for caution was suggested by Ashworth (1978) because the Moon could be a source of high-velocity craters in the μm and sub-μm sizes, which have been assumed to be from a primary source. Further, Zook et al. (1984) demonstrated that the lunar microcrater population of <7 μm pit size has been overestimated because, in these sizes, primary and high speed secondary craters cannot be distinguished.

The lunar surface had been the target for several megaimpacts with ejecta distributed over long distances. The returned lunar samples, to be reliable cosmic dust flux detectors, need to possess a 2π exposure geometry (a cratered top and a completely uncratered bottom) and an absence of a history of tumbling either in the ejecta cloud or on the surface.

CONCLUSIONS

The detailed SEM examination of microcraters on Australasian microtektites has not only shown a vast range in crater morphology but also crater geometry variation with sizes as seen on lunar samples. A large variation in crater size is seen on the microtektites from 0.3 to 600 μm, and while 2030 craters could be counted on 137 impacted microtektites, many more could have been destroyed by etching on the ocean floor. The impact energies responsible for these craters also seem to encompass a large range from the destructive effects shown by fragments, erosive impacts, and gentle accretionery impacts.

Further, small microtektites (≤450 μm) are seen to possess a large number of impacts (especially in the erosive

category), medium-sized microtektites (~450–800 µm) have a mixed population, and large microtektites (>800 µm) have very few impacts/microtektite, especially of the low-velocity variety. The apparent importance of microtektite size in collecting microimpacts seems to be due to the thermal state of the target. The larger microtektites, which cool relatively slowly, could have fragmented more easily by impacts. The impacts result from interparticle collisions that took place while the ejecta was in flight subsequent to the Australasian impact event. Apparently, these collisions could have taken place during vapor/ejecta interactions after the impact or, subsequently, during winnowing upon interaction with the atmosphere.

The lunar microcrater population shows several similarities with the data presented here in terms of the types of impacts, morphology variation with size, and crater number densities in different sizes. Therefore, to qualify as reliable cosmic dust flux detectors, the lunar samples need to satisfy stringent conditions (e.g., the absence of a history of tumbling).

Editorial Handling—Dr. Donald Brownlee

REFERENCES

Ashworth D. G. 1978. Lunar and planetary impact erosion. In *Cosmic dust,* edited by McDonnell J. A. M. New York: Wiley. pp. 427–526.

Bloch M. R., Fechtig H., Gentner W., Neukum G., and Schneider E. 1971. Meteorite impact craters, crater simulations, and the meteoroid flux in the early solar system. Proceedings, 2nd Lunar and Planetary Science Conference. pp. 2639–2652.

Brownlee D. E., Horz F., Hartung J. B., and Gault D. E. 1975. Density, chemistry, and size distribution of interplanetary dust. Proceedings, 6th Lunar and Planetary Science Conference. pp. 3409–3416.

Burns C. A. 1990. The Australasian microtektite layer: Implications concerning its source area and its relationship to the Brunhes/Matuyama geomagnetic reversal. Ph.D. thesis, University of Newark, Delaware, USA.

Carter J. L. and MacGregor I. D. 1970. Mineralogy, petrology, and surface features of some Apollo 11 samples. Proceedings of the Apollo 11 Lunar Science Conference. *Geochimica et Cosmochimica Acta* 34:247–265.

Carter J. L. and McKay D. S. 1971. Influence of target temperature on crater morphology and implications on the origin of craters on lunar glass spheres. Proceedings, 2nd Lunar and Planetary Science Conference. pp. 2653–2670.

Fechtig H., Grun E. and Kissel J. 1978. Laboratory simulation. In *Cosmic dust,* edited by McDonnell J. A. M. New York: Wiley. pp. 607–669.

Gault D. E. and Wedekind J. A. 1969. The destruction of tektites by micrometeoroid impacts. *Journal of Geophysical Research* 74: 6780–6794.

Gault D. E. and Wedekind J. A. 1978. Experimental studies of oblique impact. Proceedings, 9th Lunar and Planetary Science Conference. pp. 3843–3875.

Glass B. P. 1974. Microtektite surface sculpturing. *Geological Society of America Bulletin* 85:1305–1314.

Glass B. P. 1984. Solution of naturally-occurring glasses in the geological environment. *Journal of Non-Crystalline Solids* 67: 265–286.

Glass B. P. and Pizzuto J. E. 1994. Geographic variation in Australasian microtektite concentrations: Implications concerning the location and size of the source crater. *Journal of Geophysical Research* 99:19075–19081.

Glass B. P. and Wu J. 1993. Coesite and shocked quartz discovered in the Australasian and North American microtektite layers. *Geology* 21:435–438.

Glass B. P. and Zwart M. J. 1979. North American microtektites in DSDP cores from the Caribbean Sea and Gulf of Mexico. *Geological Society of America Bulletin* 90:595–602.

Glass B. P., Swincki M. B., and Zwart P. A. 1979. Australasian, Ivory Coast, and North American tektite strewn fields: Size, mass, and correlation with geomagnetic reversals and other Earth events. Proceedings, 10th Lunar and Planetary Science Conference. pp. 2535–2545.

Glass B. P., Chapman D. R., and Prasad M. S. 1996. Ablated tektite from the Central Indian Ocean. *Meteoritics & Planetary Science* 32:365–369.

Glass B. P., Muenow D. W., Bohor B. F., and Meeker G. P. 1997. Fragmentation and hydration of tektites and microtektites. *Meteoritics & Planetary Science* 32:333–341.

Grun E., Zook H. A., Fechtig H., and Giese R. H. 1985. Collisional balance of the meteoritic complex. *Icarus* 62:244–272.

Hartung J. B. and Horz F. 1972. Microcraters on lunar rocks. Proceedings, 24th International Geological Congress. pp. 48–56.

Hartung J. B., Horz F., McKay D. S., and Baiamonte F. L. 1972. Surface features on glass spherules from the Luna 16 sample. *Moon* 5:436–446.

Horz F. 1969. Structural and mineralogical evaluation of an experimentally produced impact crater in granite. *Contributions to Mineralogy and Petrology* 21:365–377.

Horz F., Hartung J. B., and Gault D. E. 1971. Micrometeorite craters on lunar rock surfaces. *Journal of Geophysical Research* 76: 5770–5798.

Horz F., Brownlee D. E., Fechtig H., Hartung J. B., Morrison D. A., Neukum G., Vedder J. F., and Gault D. E. 1975. Lunar microcraters: Implications for the micrometeoroid complex. *Planetary and Space Science* 23:151–172.

Horz F., Osterlag R., and Rainey D. A. 1983. Bunte breccia of the Ries: Continuous deposits of large impact craters. *Reviews of Geophysics and Space Physics* 21:1667–1725.

Horz F., Grieve R. A. F., Heiken G., Spudis P., and Binder A. 1991. Lunar surface processes. In *Lunar sourcebook: A user's guide to the Moon,* edited by Heiken G. H., Vaniman D. T., and French B. M. Cambridge: Cambridge University Press. pp. 61–120.

Le Sergeant L. B. and Lamy P. L. 1981. Collisional processes among interplanetary dust grains: An unlikely origin for the B meteoroids. *Icarus* 47:270–281.

Lorenz R. D. 2000. Microtektites on Mars: Volume and texture of distal impact ejecta deposits. *Icarus* 144:353–366.

Margolis S. V., Barnes V., Cloud P., and Fisher R. V. 1971. Surface

micrography of lunar fines compared with tektites and terrestrial volcanic analogs. Proceedings, 2nd Lunar and Planetary Science Conference. pp. 909–921.

McDonnell J. A. M. 1978. Microparticle studies by space instrumentation. In *Cosmic dust,* edited by McDonnell J. A. M. New York: Wiley. pp. 336-426.

McKay D. S., Greenwood W. R., and Morrison D. A. 1970. Morphology and related chemistry of small lunar particles from tranquility base. *Science* 167:654–656.

Melosh H. J. 1989. *Impact cratering: A geologic process.* New York: Oxford University Press. 245 p.

Melosh H. J. and Vickery A. M. 1991. Melt droplet formation in energetic impact events. *Nature* 350:494–497.

Morrison D. A. and Zinner E. 1977. 12054 and 76215: New measurements of interplanetary dust and solar flare fluxes. Proceedings, 8th Lunar and Planetary Science Conference. pp. 841–863.

Morrison D. A., McKay D. S., Fruland R. M., and Moore H. J. 1973. Microcraters on Apollo 15 and 16 rocks. Proceedings, 5th Lunar and Planetary Science Conference. pp. 3235–3253.

Neukum G., Schneider E., Mehl A., Storzer D., Wagner G. A., Fechtig H., and Bloch M. R. 1972. Lunar craters and exposure ages derived from crater statistics and solar flare tracks. Proceedings, 3rd Lunar and Planetary Science Conference. pp. 2793–2810.

Neukum G., Horz F., Morrison D. A., and Hartung J. B. 1973. Crater populations on lunar rocks. Proceedings, 4th Lunar and Planetary Science Conference. pp. 3255–3276.

Prasad M. S. and Rao P. S. 1990. Tektites far and wide. *Nature* 347: 340.

Prasad M. S. and Sudhakar M. 1996. Impact microcraters on an Australasian microtektite. *Meteoritics & Planetary Science* 31: 46–49.

Prasad M. S. and Sudhakar M. 1998. Microimpact phenomena on Australasian microtektites: Implications for ejecta plume characteristics and lunar surface processes. *Meteoritics & Planetary Science* 33:1271–1279.

Schmidt G., Zhou L., and Wasson J. T. 1993. Iridium anomaly associated with the Australasian tektite-producing impact: Masses of the impactor and of the Australasian tektites. *Geochimica et Cosmochimica Acta* 57:4851–4859.

Schneider E. and Horz F. 1974. Microcrater populations on Apollo 17 rocks. *Icarus* 22:459–473.

Schneider E., Storzer D., Hartung J. B., Fechtig H., and Gentner W. 1973. Microcraters on Apollo 15 and 16 samples and corresponding cosmic dust fluxes. Proceedings, 4th Lunar and Planetary Science Conference. pp. 3277–3290.

Schneider E., Stilp A., Bureo R., and Lambert M. 1990. Micrometeorite and space debris simulation for Columbus hull components. *International Journal of Impact Engineering* 10: 499–508.

Schultz P. H. and Gault D. E. 1985. Clustered impacts: Experiments and implication. *Journal of Geophysical Research* 90:3701–3732.

Vedder J. F. 1971. Microcraters in glass and minerals. *Earth and Planetary Science Letters* 11:291–296.

Vedder J. F. and Mandeville J. C. 1974. Microcraters formed in glass by projectiles of various densities. *Journal of Geophysical Research* 79:3247–3256.

Vickery A. M. 1986. Effect of an impact-generated gas cloud on the acceleration of solid ejecta. *Journal of Geophysical Research* 91: 14139–14160.

Zook H. A., Lange G., Grun E., and Fechtig H. 1984. Lunar primary and secondary microcraters and the micrometeoroid complex (abstract). Proceedings, 15th Lunar and Planetary Science Conference. pp. 965–966.